International Journal of Neural Systems, Vol. 26, No. 5 (2016) 1650020 (27 pages)

DOI: 10.1142/S0129065716500209

Oscillation-Driven Spike-Timing Dependent Plasticity Allows Multiple Overlapping Pattern Recognition in Inhibitory Interneuron Networks

Jesús A. Garrido*
Department of Computer Architecture and Technology
University of Granada, Periodista Daniel Saucedo Aranda s/n
Granada, 18071, Spain
jesusgarrido@ugr.es

Niceto R. Luque
Institut National de la Santé et de la Recherche Médicale
U968 and Centre National de la Recherche Scientifique
UMR_7210, Institut de la Vision, rue Moreau, 17
Paris, F75012, France

Sorbonne Universités, Université Pierre et Marie Curie Paris 06
UMR_S 968, Place Jussieu, 4
Paris, F75252, France
niceto.luque@inserm.fr

Silvia Tolu
Center for Playware, Department of Electrical Engineering
Technical University of Denmark
Richard Petersens Plads, Elektrovej, Building 326
Lyngby, Copenhagen, 2800, Denmark
stolu@elektro.dtu.dk

Egidio D'Angelo
Department of Brain and Behavioral Sciences
University of Pavia, Via Forlanini, 6
Pavia, I27100, Italy

Brain Connectivity Center
Istituto Neurologico IRCCS Fondazione Casimiro Mondino
Via Mondino, 2 Pavia, I27100, Italy
dangelo@unipv.it

Accepted 23 February 2016
Published Online 14 April 2016

The majority of operations carried out by the brain require learning complex signal patterns for future recognition, retrieval and reuse. Although learning is thought to depend on multiple forms of long-term synaptic plasticity, the way this latter contributes to pattern recognition is still poorly understood. Here, we have used a simple model of afferent excitatory neurons and interneurons with lateral inhibition, reproducing a network topology found in many brain areas from the cerebellum to cortical columns. When endowed with spike-timing dependent plasticity (STDP) at the excitatory input synapses and at the inhibitory interneuron–interneuron synapses, the interneurons rapidly learned complex input patterns.

*Corresponding author.

Interestingly, induction of plasticity required that the network be entrained into theta-frequency band oscillations, setting the internal phase-reference required to drive STDP. Inhibitory plasticity effectively distributed multiple patterns among available interneurons, thus allowing the simultaneous detection of multiple overlapping patterns. The addition of plasticity in intrinsic excitability made the system more robust allowing self-adjustment and rescaling in response to a broad range of input patterns. The combination of plasticity in lateral inhibitory connections and homeostatic mechanisms in the inhibitory interneurons optimized mutual information (MI) transfer. The storage of multiple complex patterns in plastic interneuron networks could be critical for the generation of sparse representations of information in excitatory neuron populations falling under their control.

Keywords: Spiking neural network; spike-timing dependent plasticity; intrinsic plasticity; lateral inhibition; oscillations; pattern recognition.

1. Introduction

Brain computation occurs in microcircuits made up of large numbers of excitatory and inhibitory neurons and is based on complex spike patterns generated by neurons and transmitted in the synapses. Synapses can persistently modify their efficiency in an activity dependent manner, a phenomenon called long-term synaptic plasticity, providing the basis for learning and memory.[1] In addition, synapses can also show weight rescaling mechanisms and neurons long-term changes in intrinsic excitability, all processes that may have the homeostatic role of maintaining spike discharge within certain limits.[2,3] In order to cope with real-time processing in a rapidly changing environment, the brain requires suitable neuronal coding schemes and synaptic plasticity mechanisms allowing fast and precise spike-time-correlated learning and pattern recognition. High temporal precision is therefore required both for spike timing and, consequently, for synaptic plasticity. For instance, millisecond-scale correlations among neurons in the sensorial systems are thought to improve storage capacity and computational capabilities[4,5] and long-term synaptic plasticity efficiently alters the synaptic weights to detect known stimuli (visual shapes, haptic sensations, etc.) in successive neuron layers.[6–8]

Spike-timing has long been proposed for encoding information in the brain and spike-timing dependent plasticity (STDP) to determine the weight changes required to enhance information processing. Several forms of STDP have been experimentally observed in different areas of the brain (see Ref. 9 for an extensive review). In its classical form, long-term potentiation (LTP) has been observed when a presynaptic neuron fires a spike shortly before the postsynaptic neuron, whilst long-term depression (LTD) has been measured in response to a postsynaptic spike followed by a presynaptic spike.[10–12] This kind of STDP has proved very efficient in excitatory synapses and several models implemented with this mechanism have succeeded in detecting the start of single repeated patterns in continuous spike train stimulation.[13,14] These mechanisms have been complemented with strong lateral inhibition, allowing multiple nonoverlapping patterns to be detected in multi-neuronal networks in a *winner-takes-all* scheme.[15]

Inhibitory synapses have also been experimentally shown to express a particular type of symmetric STDP in the hippocampus[11,16] and the auditory cortex.[17] In these cases, LTP is induced when presynaptic and postsynaptic spikes occur in close time vicinity, irrespective of the reciprocal order, whilst LTD is induced when the presynaptic and postsynaptic spikes occur further away in time, with distances ranging from between 40 ms and 100 ms. Theoretical studies have recently hypothesized the role of inhibitory STDP in the interneuron synapses, pointing mainly in two directions: (i) balancing excitation and inhibition in feed-forward inhibitory loops,[18,19] and (ii) decorrelating the activity of its corresponding excitatory neuron population and producing sparse recoding of the sensory signals.[20] However, the influence of additional factors (namely, the spike triplet interactions, the postsynaptic firing frequency or the axonal delays)[21,22] as well as the role of inhibitory STDP in brain information processing still remains unclear.

Since the real world is continuously evolving and the information flow fluctuates, biological systems have developed homeostatic mechanisms to counteract the effects of changes, maintaining levels of

activity stable within convenient ranges.[23] While Hebbian learning seems to modify synaptic weights in order to store information in the network, at longer time scales synaptic rescaling[24] readjusts the weights in a non-specific way. Finally, experimental evidence indicates that intrinsic plasticity mechanisms modify the excitability of the neurons in order to adapt the behavior to changing levels of synaptic input in several brain areas (e.g. in the visual cortex,[25] ganglion neurons[26]; see Ref. 23 for an in-depth review). The joint operation of all these mechanisms keeps the network stable with no information loss.[27]

The interplay between long-term synaptic plasticity and homeostatic mechanisms has recently been reviewed.[28] From a practical point of view, the dynamic nature of the real world remarkably affects neural information processing. A typical issue with networks incorporating STDP learning rules is the tedious tuning needed to adjust their parameters in order to cope with the current conditions of the networks. Indeed, small changes in network conditions (including number of inputs, number of outputs, firing rate of the inputs, correlation of the activity...) tend to destabilize the learning process, even in the case of supervised learning, requiring a fine readjustment of the parameters to the new conditions.[29–31] The introduction of homeostatic and synaptic rescaling processes should automatically prevent the problem.

Spiking neural networks have long been proposed to solve different problems involving learning, such as classification[32,33] or combinatorial optimization.[34] However, the way information is encoded in the spiking activity of a neuronal population is also critical to the way a system learns new information.[35–37] Several alternatives have been suggested in order to enable sparse coding in spiking neural network populations, such as radial-basis function encoding in early sensorial layers[35] and locally competitive algorithms.[38] Thus, biologically plausible learning rules such as STDP can play a major role in providing sparse representations of the sensorial information. Although STDP rules use the time difference between presynaptic and postsynaptic activity to potentiate or depress the synapses, its usage is not restricted to patterns defined in the spike time. In this sense, oscillations in the local field potential have been proposed to transform firing rate patterns from the sensorial pathways into phase-of-firing coding compatible with STDP learning rules.[14] According to this study, combining an oscillatory input current with stimulus-dependent static components (including current combination patterns) produces variations in both the phase of firing and the firing rate that depend on the current of the particular stimulus. Indeed, these coding mechanisms implemented in a population of converging neurons have been demonstrated to enable a target neuron to recognize and detect the presence of a repetitive current pattern stimulating the input population,[14] enhancing the unsupervised learning capabilities of spiking neural networks.[39] In addition, a recent theoretical work has revealed the importance of intrinsic neural resonance and bursting to enhance the transmission of the signal in connections equipped with STDP.[40]

Aiming to dissociate the effect that each of the aforementioned mechanisms plays in learning we have constructed a spiking network model of inhibitory interneurons with lateral inhibition. This network has been equipped with excitatory (eSTDP) and inhibitory (iSTDP) spike-timing dependent plasticity and with homeostatic mechanisms (namely, intrinsic plasticity and synaptic weight scaling). The network is then stimulated by repetitive patterns (consisting of different values of current targeting each of the input-layer neurons involved) over background noise. After 25 min of continuous stimulation of background noise and correlated input current levels the inhibitory interneurons were responsive to the presentation of the different patterns. The efficacy of the recognition and detection was quantified in terms of information transmission.

iSTDP effectively improved the learning capabilities of the network by increasing the lateral inhibition strength during the beginning of the learning and reducing it once each inhibitory neuron had become sensitive to a different pattern. On the other hand, homeostatic mechanisms made the network more robust to changes in the learning parameters and allowed the effective detection of patterns independently of the number of afferent neurons included in it. Therefore, distributed plasticity can implement a flexible control over information transmission, even in simple inhibitory interneuron networks, with potentially important implications for brain functioning.

2. Methods

To prove the learning capabilities of eSTDP and iSTDP mechanisms a recurrent spiking neural network has been implemented. It consists of excitatory afferent neurons (named excitatory or afferent neurons for simplicity) that converge on a population of target interneurons (named inhibitory or target neurons for simplicity) generating lateral inhibition as shown in Sec. 2.1.

The afferent layer of our network conveys partially-overlapped patterns that are generated over background noise (see Sec. 2.2). The network input layer is stimulated for 1500 s and the mutual information (MI) between the input pattern sequence and the activity at the inhibitory population (see Sec. 2.3) is calculated for the last 200 s. The MI gives a specific and quantifiable measurement of the learning capability of the network. Finally, for each of the studied network settings, the parameter space of the learning rules (namely, eSTDP and iSTDP) has been exhaustively explored as shown in Sec. 2.4.

2.1. *The network structure*

Figure 1(a) shows the structure of the network implemented in this model. It includes 2000 afferent excitatory neurons converging to a reduced population of inhibitory interneurons (accounting for a variable number of neurons depending on the particular experiment). Every excitatory neuron connects all the inhibitory interneurons. The inhibitory interneurons, in turn, inhibit all the other inhibitory neurons. This is the simplest structure allowing the study of the complementary roles that excitatory and inhibitory STDP plays when repeated patterns are presented to the input neurons.

2.1.1. *The neuron and synapse models*

Excitatory input neurons were modeled using current-based versions of the LIF model[41] (see Appendix A.1 for further details on the equations and neurons parameters).

Intrinsic plasticity processes have recently been shown to modify the excitability of the neurons to adapt the neuron behavior to changing levels of synaptic input received.[23,25,26] Inhibitory neurons were modeled using a conductance-based version of the LIF model (the general equations of this model are included in Appendix A.1) including intrinsic plasticity.[42] To the best of our knowledge, this is the only LIF model in the literature integrating intrinsic plasticity properties.

Additionally, the intrinsic plasticity has been modeled by updating the inverse value of the membrane capacitance (r_C) and the leak conductance (g_{leak}) as proposed in Ref. 42 according to the following differential equations:

$$\frac{dg_{\text{leak}}}{dt} = -\frac{(-g_{\text{leak}} - \beta)}{\tau_{\text{IP}}}, \tag{1}$$

$$\frac{dr_C}{dt} = \frac{\frac{1}{r_C} + \beta \cdot I_{\text{syn}}}{\tau_{\text{IP}}}, \tag{2}$$

where τ_{IP} is the intrinsic plasticity time constant and has been set to 12,000 s and β is a parameter controlling the shape of the firing rate distribution and it has been set to 0.8. The τ_{IP} value has been chosen after preliminary simulations maintaining the amount of LTP fixed within the eSTDP mechanism (see $A^{\text{LTP}}_{\text{eSTDP}}$ parameter in Appendix A.2). This value is high enough to prevent interferences between the intrinsic plasticity and the STDP mechanisms during the learning process and is low enough to prevent silent neurons for long periods.

Finally, since the intrinsic plasticity mechanism aims to regulate the neuronal firing rate, each time the neuron elicits a spike the r_C and g_L variables are modified according to the following equations:

$$\Delta r_C = -\frac{\varepsilon_{r_C} \cdot (1+\beta) \cdot I_{\text{syn}}}{\tau_{\text{IP}}}, \tag{3}$$

$$\Delta g_{\text{leak}} = \frac{\varepsilon_{g_{\text{leak}}} \cdot (1+\beta)}{\tau_{\text{IP}}}, \tag{4}$$

where ε_{rC} and $\varepsilon_{\text{gleak}}$ control how each elicited spike influences the membrane capacitance and leak conductance, respectively. These constants have been set to $34.55\text{F}\cdot\text{s/A}$ and $4923.88\text{S}\cdot\text{s}$ to make the neuron fire with low activity levels (around 1 Hz). These values were obtained using bidimensional exhaustive exploration (logarithmic scale) of the firing rate with stimulation patterns similar to the ones used in this study. The selected combination of values will lead the neuron to fire at low (but not too low) firing rates. The r_C and g_{leak} variables have been initialized to $1/50\,\text{F}^{-1}$ and $1/3\,\text{nS}$.

Figure 1(b) shows an example of how this neuronal mechanism can adapt the electrical properties of the neuron to keep its firing rate stable throughout the simulation. In order to show the stability of

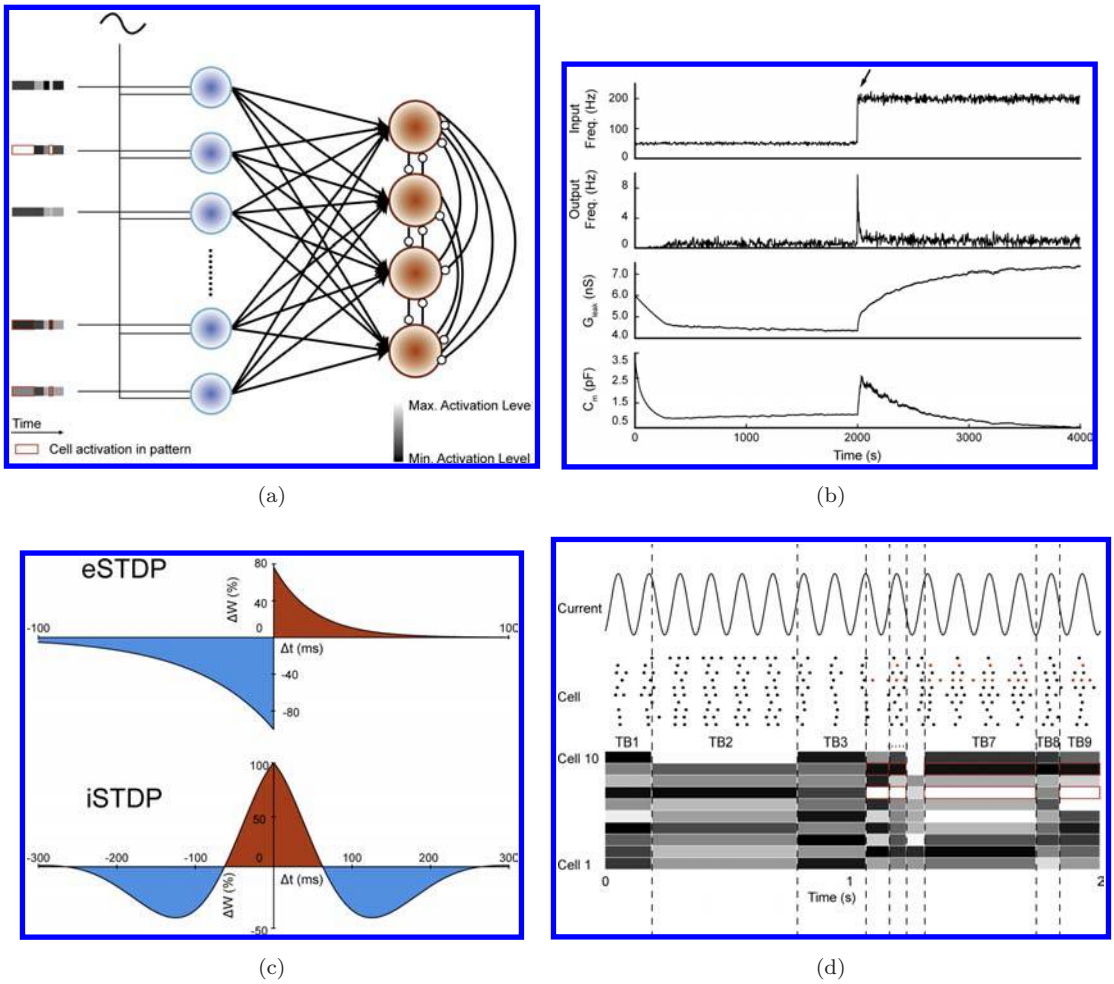

Fig. 1. (Color online) Schematic drawing of the simulated network, stimulation protocols and plasticity mechanisms. (a) Neural network structure studied. 2000 excitatory neurons (blue circles) receive external stimulation composed of a carrier 8 Hz oscillatory signal in addition to randomly generated input combinations (embedding the presented patterns). These neurons make excitatory synapse (with eSTDP, arrow-ending connectors) with the inhibitory cells (red circles) presenting lateral inhibition (with iSTDP —circle-ending connectors). (b) Example simulation showing the operation of the intrinsic plasticity mechanism implemented in the inhibitory neurons. Note the output frequency (medium–high) adaptation in response to the increase of the input frequency (top) occurring at 2000 s (marked with an arrow). After the leak conductance (mid–bottom) and the membrane capacitance parameters have evolved, the output frequency tends to stabilize around 1.5 Hz. (c) Representation of the excitatory (eSTDP, top) and inhibitory (iSTDP, bottom) STDP learning rules. Blue areas represent LTD while red areas indicate LTP. (d) The external stimulation targeting the excitatory neurons is composed of an 8 Hz oscillatory signal (top) in addition to randomly generated input combinations (bottom) (embedding the presented patterns —red rectangles) for each time-bin (TB). These two signals force each excitatory neuron to elicit between one and three spikes for each oscillatory cycle as shown in the 2 s raster plot (middle). The pattern-generated spikes are represented by red dots while the background-generated spikes are in black.

the intrinsic plasticity mechanism the time constant (τ_{IP}) was set to 1200 s (10 times faster than in the rest of the simulations in the paper). In this simulation, a single neuron (with only one synaptic input) was set to receive 50 Hz input stimulation for the initial 2000 s and 200 Hz stimulation for the remaining 2000 s (top row). In response to this stimulation, a neuron equipped with intrinsic plasticity adapted its firing rate, being on average 0.70 Hz during the low-input-rate half and 1.3 Hz during the high-input-rate half (second row). Interestingly, at the beginning of the simulation the neuron was almost silent, and right after the change of the input rate (arrow) the neuron reached a peak of 9 Hz. However, the

output-firing rate became stable around 1 Hz after several hundred of seconds' simulation due to the adaptation of the leak conductance and the membrane capacitance.

2.1.2. *Spike-Time dependent plasticity*

The weights of the excitatory synapses (those connecting the stimulation fibers with the inhibitory neurons) have been implemented following classical additive excitatory spike-time dependent plasticity (eSTDP)[41] (see Appendix A.2).

Hebbian plasticity has been shown to result in uncontrolled weight growth, producing in certain cases a lack of selectivity in the receptive fields.[23] In order to avoid this undesired behavior, two homeostatic mechanisms have been added to the excitatory synapses. On the one hand, synaptic weights have been bounded between 0 and $\text{MaxWeight}_{\text{eSTDP}}$, avoiding that these potentiated connections rise indefinitely. On the other hand, synaptic scaling[24] has been implemented in the excitatory synapses so that the weights of all those connections targeting every neuron will be proportionally adjusted to add up to 40 nS after every second of simulation.

The inhibitory synapses implement a particular type of symmetric STDP (iSTDP) that neglects the order in which presynaptic and postsynaptic spikes occur. As shown in Fig. 1(c) this learning rule will produce LTP when a presynaptic spike is fired closely before or after a postsynaptic spike. Meanwhile, LTD will be produced when presynaptic and postsynaptic spikes occur uncorrelated (far away in time). The equation governing the iSTDP learning rule is the following:

$$\begin{aligned}\Delta w = \frac{1}{2} \cdot \Bigg(& A^{\text{LTP}}_{\text{iSTDP}} \cdot e^{-\frac{|t_{\text{pre}} - t_{\text{post}}|}{\tau^{+}_{\text{iSTDP}}}} \\ & \cdot \left(1 + \cos\left(2 \cdot \frac{t_{\text{pre}} - t_{\text{post}}}{\tau^{+}_{\text{iSTDP}}}\right)\right) \\ & - A^{\text{LTD}}_{\text{iSTDP}} \cdot C \cdot e^{-\frac{|t_{\text{pre}} - t_{\text{post}}|}{\tau^{-}_{\text{iSTDP}}}} \\ & \cdot \left(1 - \cos\left(2 \cdot \frac{t_{\text{pre}} - t_{\text{post}}}{\tau^{-}_{\text{iSTDP}}}\right)\right)\Bigg). \end{aligned} \tag{5}$$

This formula establishes the iSTDP as the difference between two exponential functions, emulating the Mexican-hat shape that has been observed in experimental results of inhibitory synapse learning rules.[43] The cosine terms make the exponential functions more timely correlated as shown in Fig. 1(c), avoiding distant pre/post-synaptic spikes affecting each other. Similarly to the eSTDP rule, τ^{+}_{iSTDP} and τ^{-}_{iSTDP} are the time constants of the potentiation and depression components and have been set to 125 ms and 195.6 ms, respectively. According to these values, they will potentiate those synapses connecting two neurons that tend to fire within the same oscillatory cycle (see stimulation section below) and inversely, those neurons firing in contiguous oscillatory cycles will be depressed.

The maximum amount of LTP ($A^{\text{LTP}}_{\text{iSTDP}}$) (occurring in response to a pair of coincident presynaptic and postsynaptic spikes) has been set to $A^{\text{LTP}}_{\text{iSTDP}} = 30.0 \cdot 10^{-3} \cdot \text{MaxWeight}_{\text{iSTDP}}$, whilst the maximum amount of LTD has been adjusted in relation to the amount of LTP according to $A^{\text{LTD}}_{\text{iSTDP}} = r^{\text{LTD/LTP}}_{\text{iSTDP}} \cdot A^{\text{LTP}}_{\text{iSTDP}}$. Similarly to the eSTDP rule, the influence of $\text{MaxWeight}_{\text{iSTDP}}$ and $r^{\text{LTD/LTP}}_{\text{iSTDP}}$ parameters in the information transmission has been studied throughout the result section. Finally, the constant C has been set to 5.0451 to normalize the relative influence of the LTD in relation to the LTP.

The network model has been implemented using the NEST 2.4.2 simulator.[44] Differential equations were solved using a Runge–Kutta–Fehlberg numeric method with an integration fixed time step dt of 100 μs.

2.2. *Pattern generation and stimulation paradigm*

In order to test the learning capabilities of the network an extension of the benchmark previously proposed in Ref. 14 has been designed. The benchmark in Ref. 14 measures the capability of a single neuron to detect the existence of one pattern of correlated input activation levels involving an unknown subset of the afferents. Both the duration of the patterns occurrences and the interval at which the pattern is presented are unpredictable. In this paper, we have extended this benchmark to allow more than one different pattern to be presented and partially overlap with each other.

Similarly to the way it was implemented in Ref. 14, a stimulation matrix is randomly generated, corresponding to the normalized activation levels. Each row of the matrix represents one afferent cell,

while each column symbolizes the activation pattern for each time column, where the lengths are randomly extracted from an exponential distribution with average 25 ms. Therefore, all the afferent neurons change their activation level at the same time (according to the duration of that particular time column) as shown in Fig. 1(d).

Each stimulation pattern has been randomly extracted from this stimulation matrix. We want to clarify at this point that in this study an input pattern represents a combination of input current values conveyed to a set of input neurons, but not the sequence of spikes fired by those neurons. Unless differently stated, 10% of the neurons are randomly chosen to be part of each pattern. A random column of exactly these neurons is selected and replicated to 20% of the time columns. In case, two or more patterns have to be generated in the same time column a random permutation defines the priority between the overlapped patterns in those afferents which are common to several patterns. Thus, the first pattern in that permutation will be presented complete throughout all its associated afferents during the time column, the second pattern will be presented only throughout those which are not included in the first pattern, and so on. However, this priority is again, randomly generated for successive time columns. This design emulates the way in which opaque objects hide other backward objects in natural scenes.

Once all the patterns have been replicated throughout the whole simulation time, both the rows and the columns of the activation matrix are iteratively normalized, aiming to keep the time-averaged and population-averaged activation levels constant throughout the simulation.

Finally, the matrix activation levels were transformed into spike activity by means of the 2000 current-based LIF afferent neurons. These cells were set to receive the input currents according to the activation matrix added to a common sinusoidal signal according to the following equation:

$$I_e(t) = \frac{A}{2} \cdot \sin(2 \cdot \pi \cdot f \cdot t - \pi) + \mathrm{Act}(t) \cdot (\mathrm{MaxAct} - \mathrm{MinAct}) + \mathrm{MinAct}, \quad (6)$$

where $I_e(t)$ is the total excitatory current stimulating the afferent neuron (see Eq. (A.1) in Appendix A), $A = 0.15\,\mathrm{pA}$ is the amplitude of the oscillatory signal, $f = 8\,\mathrm{Hz}$ is the frequency of the oscillation, $\mathrm{Act}(t)$ is the normalized level of activation extracted from the activation matrix, and $\mathrm{MaxAct} = 1.15\,\mathrm{pA}$ and $\mathrm{MinAct} = 0.90\,\mathrm{pA}$ are the maximum and minimum levels of currents corresponding to the activation levels of the matrix. These values were chosen to ensure that every afferent neuron fires between one and three spikes within a single oscillatory cycle.

1500 s simulations have been run. During the entire simulation, the network has been exposed to both the input patterns and a random background activity (according to the matrix commented above) all being modulated by an oscillatory signal. For the last 200 s, the stimulation patterns and the response of the interneuron population have been recorded and analyzed in order to extract the amount of transmitted information.

2.3. *Analysis of simulated results: Mutual information*

Following the benchmark proposed in Ref. 14 the pattern recognition accuracy was estimated by using information theory. The simulation time was discretized with 125 ms bins (the same length of the oscillatory cycles). A pattern was considered to occur in a TB if, and only if, it was present for at least half of the bin length. Then, all the combinations of patterns (each one being present or not) were considered as the possible states of the stimulation (S), while all the combinations of the inhibitory neuron activity (each neuron firing or not) were considered as the possible states of the response (R). The MI[14,45] between the neuron population activity and the stimulation patterns was calculated according to the following formula:

$$\mathrm{MI} = H(S) + H(R) - H(S,R), \quad (7)$$

where $H(S)$ is the entropy of the stimuli, $H(R)$ the entropy of the responses and $H(S,R)$ the joint entropy of the stimuli and the responses and are defined as follows:

$$\begin{aligned} H(S) &= -\sum_{s \in S} P(s) \cdot \log_2(P(s)), \\ H(R) &= -\sum_{r \in R} P(r) \cdot \log_2(P(r)), \\ H(S,R) &= -\sum_{s \in S} \sum_{r \in R} P(s,r) \cdot \log_2(P(s,r)), \end{aligned} \quad (8)$$

where S is the set of all the possible combinations of presence/absence of input patterns and R is the set of all the possible combinations of firing/silence of the inhibitory neurons. P represents the estimation of the probability of occurrence of the stimulus combinations, the response combinations or both simultaneously. This estimate has been calculated considering the last 200 s of the simulation.

A perfect detector would present $H(S) = H(R) = H(S,R)$, and the upper bound of the MI would be $\mathrm{MI}_{\max} = H(S)$. Our aim is to study the scalability of our network model according to the increasing number of patterns to be identified. The ratio between the MI and the maximal MI gives us a normalized estimator for quantifying the learning capability of our model.[46] Therefore, the uncertainty coefficient (UC) has been defined as follows:

$$\mathrm{UC} = \frac{\mathrm{MI}}{\mathrm{MI}_{\max}} = \frac{H(S) + H(R) - H(S,R)}{H(S)}, \quad (9)$$

where MI represents the actual mutual information obtained with the network at the end of the simulation and $\mathrm{MI}_{\max}$ is the maximum mutual information that could be reached with that particular stimulation. Therefore, a perfect detector would obtain $\mathrm{UC} = 1$.

2.4. *Parameter fitting with exhaustive exploration*

As commented above, two parameters of each learning rule have been adjusted in order to determine the recognition capabilities of the network. Namely, $\mathrm{MaxWeight}_{\mathrm{eSTDP}}$, $r^{\mathrm{LTD/LTP}}_{\mathrm{eSTDP}}$ have been exhaustively explored by using tridimensional figures mapping the setting values and the UC obtained with such a configuration. Once the best eSTDP setting has been obtained and fixed in the network, the iSTDP parameters ($\mathrm{MaxWeight}_{\mathrm{iSTDP}}$ and $r^{\mathrm{LTD/LTP}}_{\mathrm{iSTDP}}$) have been explored following the same procedure. This exploration strategy allows us to gain a graphical view of the influence that each parameter has in the pattern recognition accuracy of the network.

However, multidimensional evolutionary algorithms have also been used to rule out any dependence amongst eSTDP, iSTDP, and intrinsic plasticity parameters. The average UC, with 20 different seeds, was used as the fitness function of the algorithm. Each individual consisted of the eSTDP ($\mathrm{MaxWeight}_{\mathrm{eSTDP}}$ and $r^{\mathrm{LTD/LTP}}_{\mathrm{eSTDP}}$), the iSTDP ($\mathrm{MaxWeight}_{\mathrm{iSTDP}}$ and $r^{\mathrm{LTD/LTP}}_{\mathrm{iSTDP}}$), and the intrinsic plasticity parameters ($\varepsilon_{\mathrm{rC}}$, $\varepsilon_{\mathrm{gleak}}$ and τ_{IP}). The crossover operator permuted one of the parameters between the selected individuals whereas the mutation operator set one of the parameters to a new random value. The best individuals were similar to those obtained with the bidimensional exhaustive exploration.

In order to avoid a particular seed (used to generate both the stimulation current sequence and the initial weights of the network) influencing the parameter fitting procedure, 20 simulations (with different seeds) have been run with each parameter set, and the average of the UC has been used to select the optimal configuration. Finally, aiming to validate the results of the fitting procedure and a fair comparison of different networks, the selected setting has been tested over a fully different set of 250 fixed seeds.

This algorithm was implemented in Python, calling the NEST Python interface[47] and was executed in parallel at the Alhambra cluster at the University of Granada by using 128 cores (for each execution of the parameter exploration algorithm).

3. Results

We have reproduced the results reported in Ref. 14 as starting point. In this study, a single target neuron was able to recognize one pattern when it was presented to the input layer (Sec. 3.1). We have added to this initial network configuration a second target neuron and an additional overlapped input pattern (Sec. 3.2). Finally, we have scaled the number of patterns, target neurons (Sec. 3.3) and inhibitory neurons per pattern (Sec. 3.4) model. This scaling allowed us to extend the role of the lateral inhibition and iSTDP in model learning. Finally, modifying the number of inputs involved in the pattern allowed us to quantify the impact of intrinsic plasticity and weight scaling in the model learning capabilities (Sec. 3.5).

3.1. *Single pattern recognition with eSTDP*

As a first step, we reproduced the results previously reported in Ref. 14, in which a similar network including 2000 afferent neurons and a single

target neuron that was able to detect the occurrence of a single pattern only. After exhaustive exploration of the eSTDP parameter space (including $\text{MaxWeight}_{\text{eSTDP}}$ and $r_{\text{eSTDP}}^{\text{LTD/LTP}}$ parameters, since no lateral inhibition is included with only one target neuron), the network managed to recognize when the pattern was presented with similar accuracy as in Ref. 14. At the beginning of the simulation (Fig. 2(a), left), the target neuron remained silent due to the parameters set for the neuron model (namely, inverse of membrane capacitance, r_C and leak conductance, g_L) and the weights of the excitatory connections. However, due to the low initial firing rate of the target neuron, the intrinsic plasticity mechanism reduces r_C and g_L and the neuron starts firing unselectively after 200 s (Fig. 2(a), middle), eliciting singlets or doublets every oscillatory cycle.

Once the target neuron starts firing, the eSTDP mechanism adjusts the excitatory weights, potentiating those connections whose presynaptic spikes frequently happen right before the postsynaptic spike. This mechanism drives the postsynaptic neuron to nearly perfect recognition of the pattern (Fig. 2(a), right) after 600 s of simulation and remains stable from that moment. Thus, at the end of the simulation time, the target neuron fires only in response to the presentation of the pattern in the afferent neurons. The eSTDP mechanism strengthens those connections whose afferent neurons are included in the pattern and whose activation levels make them fire before the postsynaptic firing phase (Fig. 2(b)), whilst decreasing the remaining connections. In particular, those synapses involving afferent neurons with activation levels ranging between 0.25 and 0.6 (Fig. 2(b)), become potentiated. As expected, the afferent neurons corresponding to those connections tend to fire (when the pattern is presented to the network) some

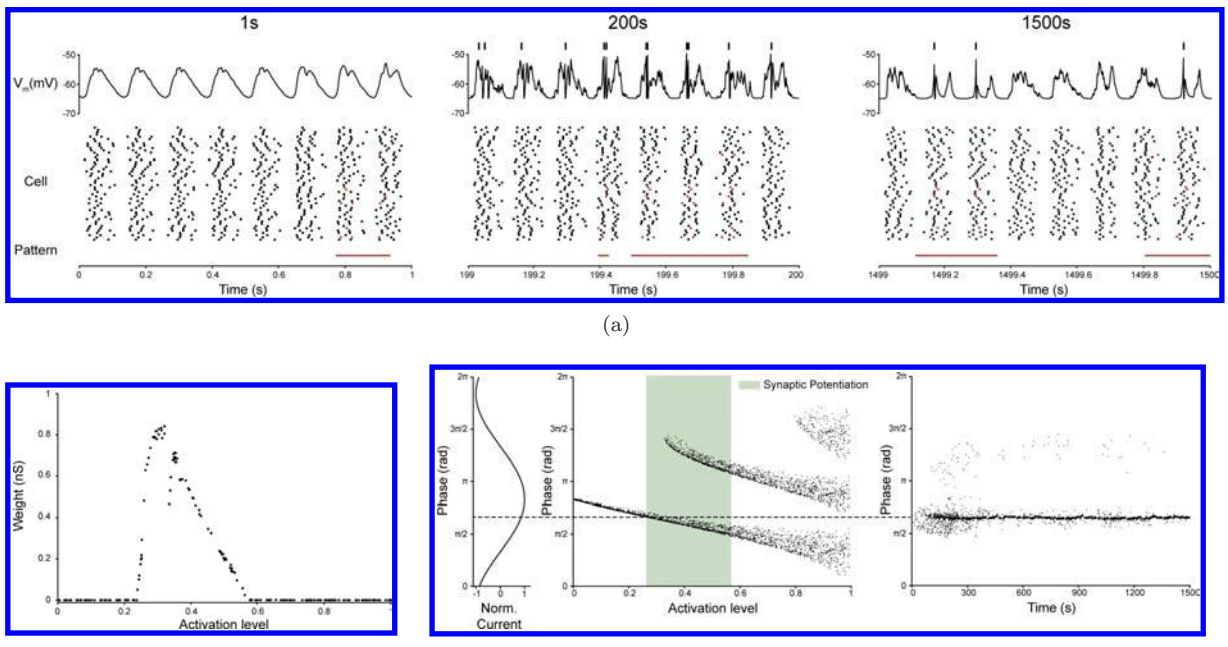

Fig. 2. (Color online) Learning with one target neuron and one pattern. (a) Membrane potential of the target neuron (top) and a raster plot of 50 randomly chosen excitatory neurons (middle). The red lines at the bottom represent when the pattern is presented to the afferent neurons. The activity at 1 s (left), 200 s (middle) and 1500 s (right) is shown. The vertical bars over the membrane potential lines indicate the occurrence of inhibitory spikes. (b) Normalized excitatory synaptic weights after 1500 s of simulation as a function of the activation level of the corresponding afferent neuron during presentation of the pattern. (c) Normalized oscillatory current conveyed to all the afferent neurons (left). Afferent neuron firing phase as a function of the activation level during an oscillatory cycle (middle). Note that firing phase slightly shifts due to the variability in the initial membrane potential of each afferent neuron. The green box represents the activation levels that are not depressed at the end of the learning as represented in (b). Target neuron firing phase during a 1500 s simulation (right).

milliseconds earlier than the peak of the input oscillation (≈2.08 rad) (Fig. 2(c), left and middle). Similarly, target neuron firing evolves from unpredictable phase mainly during the near-the-top range at the beginning of the learning process to precise firing occurring at around 2.08 rad at the end of the simulation (Fig. 2(c), right).

3.2. *Multiple pattern recognition with eSTDP and iSTDP*

Once the network and its plasticity mechanisms had been shown to recognize complex patterns, we wondered whether a network including several inhibitory neurons connected with synapses implementing iSTDP would be able to recognize multiple partially overlapping patterns. In order to test this hypothesis, a second neuron was added to the network and inhibitory synapses equipped with iSTDP were set reciprocally connecting each target neuron. In addition to this, two randomly chosen patterns were inserted over the background noise and the network simulation was allowed to run for 1500 s.

Similarly to the case with only one pattern, at the beginning of the simulation the two inhibitory neurons remain silent (Fig. 3(a), left) until their intrinsic plasticity modifies the electrical properties of the neurons to increase the average firing rate. At the end of the simulation, each one of the target neurons becomes responsive to one of the patterns (Fig. 3(a), right) and fires if and only if its corresponding pattern is presented to the afferent neurons. Interestingly, even in those oscillatory cycles in which the two patterns were simultaneously presented the two inhibitory neurons fire, enabling stimulation patterns to be detected independently of the presence of the

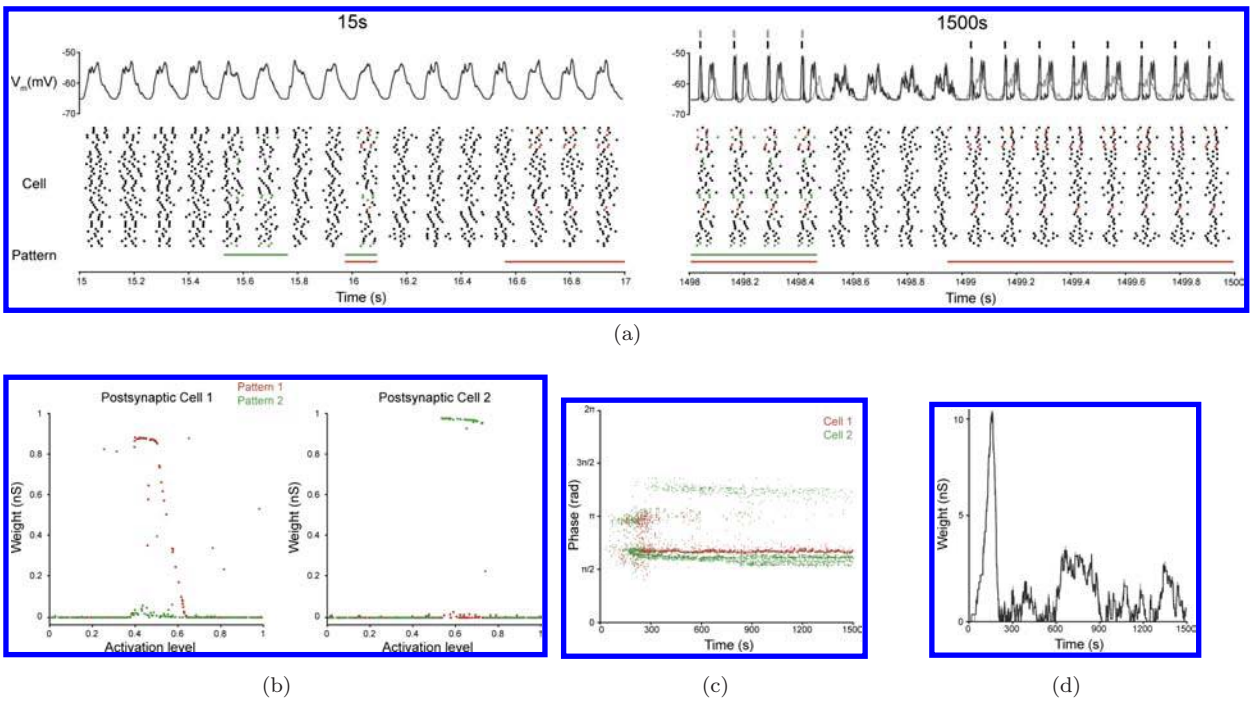

Fig. 3. (Color online) Learning with two inhibitory neurons and two patterns. (a) Membrane potential traces of the inhibitory neurons (top, black and gray traces) and a raster plot of 50 randomly chosen afferent neurons (middle). The red and green lines at the bottom represent when patterns one and two are presented to the afferent neurons. The 2 s activity after 15 s (left) and 1498 s (right) of simulation are shown. The vertical bars over the membrane potential lines indicate the occurrence of spikes in inhibitory neurons one (black) and two (gray). Note that inhibitory neuron one becomes responsive to pattern one while inhibitory neuron two becomes responsive to pattern two. (b) Normalized excitatory synaptic weights after 1500 s of simulation as a function of the activation level of the corresponding afferent neuron in each presented pattern (pattern one red, pattern two green). Representation of the synapses targeting the inhibitory cells one (left) and two (right). (c) Inhibitory neuron firing phase during a 1500 s simulation. (d) Evolution of the inhibitory synaptic strengths (connecting the inhibitory neurons one with each other) during the simulation. Note that two traces overlap (black and gray) but they have similar values almost all the time due to the symmetric iSTDP.

other pattern (contrary to what occurs in *winner-takes-all* networks[15]).

Figure 3(b) represents the synaptic weights between the afferent neurons included in each pattern (represented as its activation level) and the target neurons. It evidences that eSTDP potentiates connections included in pattern one (with activation levels ranging between 0.4 and 0.6) and targeting inhibitory neuron one (Fig. 3(b), left), and those connections included in pattern two (with activation levels between 0.5 and 0.7) and targeting inhibitory neuron two (Fig. 3(b) right). All the remaining synapses were depressed. According to these results, the eSTDP learning rule will either punish or reward by either increasing or decreasing the weights associated to certain activation levels depending on: (i) the ratio between maximum LTP and LTD (the $r_{\text{eSTDP}}^{\text{LTD/LTP}}$ parameter), and (ii) the offset of each presynaptic spike occurring during pattern presentation. The combination of these factors will define the range for the potentiated activation levels and the offset of the inhibitory spike (Fig. 3(c)). The activation levels potentiated by eSTDP might become different depending on the actual sampled patterns and the $r_{\text{eSTDP}}^{\text{LTD/LTP}}$ (compare the weights between Figs. 2(d) and 3(b)).

This combination of synaptic weights and activation levels drives the target neurons to fire in response to their corresponding patterns with different phases (around 2.03 rad for the first target neuron — responsive to the first pattern and 1.88 rad for the second target neuron — responsive to the second pattern) (Fig. 3(c)). Indeed, the final configuration of weights frequently conducts the second target cell to elicit a second spike (doublet) (around 3.82 rad phase) in response to the second pattern (Fig. 3(c)).

Finally, this simple example allowed us to qualitatively show the operation of the iSTDP mechanism in the inhibitory synapses between target neurons (Fig. 3(d)). When the target neurons start firing unselectively (between 0 s and 200 s) the inhibitory weights of these connections are increased due to the highly-correlated firing between the two target neurons. As a consequence of the weight increase, the reciprocal inhibition reduces the probability of both neurons to fire in the same oscillatory cycle (or respond to the same pattern), leading every target neuron to become specialized in a different pattern. Therefore, the activity of the two target neurons becomes less correlated, and the iSTDP rule depresses the weights of both inhibitory synapses (between 200 s and 300 s). From then on, the iSTDP learning rule keeps the inhibitory weights low until the end of the simulation.

3.3. *Multiple pattern scalability with eSTDP and iSTDP*

Once our simple network including eSTDP and iSTDP proved able to recognize two random patterns presented to the input cells, we wondered whether this system scales up to recognize more than two patterns and how the learning rule parameters need to be modified for successful learning in each particular case. Therefore, we have explored the learning parameter space independently for eSTDP parameters ($\text{MaxWeight}_{\text{eSTDP}}$ and $r_{\text{eSTDP}}^{\text{LTD/LTP}}$) and iSTDP parameters ($\text{MaxWeight}_{\text{iSTDP}}$ and $r_{\text{iSTDP}}^{\text{LTD/LTP}}$) by using a network including four target cells and being stimulated with four patterns inserted over background noisy activity. The best configuration (in terms of average UC) has been found with $\text{MaxWeight}_{\text{eSTDP}} = 1.1\,\text{nS}$ and $r_{\text{eSTDP}}^{\text{LTD/LTP}} = 1.1$ (Fig. A.1(a), left), $\text{MaxWeight}_{\text{iSTDP}} = 11.9\,\text{nS}$ and $r_{\text{iSTDP}}^{\text{LTD/LTP}} = 0.552$ (Fig. A.1(b), left).

After 512 repetitions with the same network and learning rule parameters but different initialization seeds, simulations yield average UC $= 0.53 \pm 0.098$. Interestingly, the range of eSTDP parameters with high UC (above 0.5) was rather wide ranging from $\text{MaxWeight}_{\text{eSTDP}} = 0.5\,\text{nS}$ up to the $\text{MaxWeight}_{\text{eSTDP}} = 3.0\,\text{nS}$ (maximum explored value) and from $r_{\text{eSTDP}}^{\text{LTD/LTP}} = 1.0$ up to $r_{\text{eSTDP}}^{\text{LTD/LTP}} = 1.8$. On the other hand, those iSTDP parameters ranging from $r_{\text{iSTDP}}^{\text{LTD/LTP}} = 0.40$ to $r_{\text{iSTDP}}^{\text{LTD/LTP}} = 0.60$ yield high UC (assuming nonnegligible $\text{MaxWeight}_{\text{iSTDP}}$). High values of $\text{MaxWeight}_{\text{iSTDP}}$ require higher $r_{\text{iSTDP}}^{\text{LTD/LTP}}$ values, whilst the low values of $\text{MaxWeight}_{\text{iSTDP}}$ need to be compensated by lower $r_{\text{iSTDP}}^{\text{LTD/LTP}}$ values. As far as the coefficient of variation (CV) is considered, those areas with high UC also present lower CV values (right column in Fig. (A.1) and A.1(b)), indicating that most of the patterns were frequently recognized with high accuracy by those configurations.

Similarly to the iSTDP configuration, the space of parameters has been explored for (i) the network including eSTDP and fixed inhibition (instead

of iSTDP) and (ii) the network including no inhibition between the target neurons. In the first case, the best configuration is obtained with $\text{MaxWeight}_{\text{eSTDP}} = 1.2\,\text{nS}$, $r_{\text{ieTDP}}^{\text{LTD/LTP}} = 1.3$ (Fig. A.2(a)) and inhibitory synapses set to 1.8 nS (Fig. A.2(b)). This configuration drives the network to perform with UC $= 0.49 \pm 0.10$ (Fig. 4(a)). The network with no inhibition obtains its best accuracy with $\text{MaxWeight}_{\text{eSTDP}} = 1.1\,\text{nS}$ and $r_{\text{eSTDP}}^{\text{LTD/LTP}} = 1.7$ (Fig. A.3(a)), with UC $= 0.40 \pm 0.12$. Therefore, when the afferent neurons receive four different patterns the network with iSTDP between the target neurons outperforms (on pattern recognition accuracy) the one with fixed lateral inhibition and the counterpart with no inhibition at all.

In order to verify how the proposed networks scale up with the number of patterns, the three configurations (with iSTDP, fixed-weight lateral inhibition or with no lateral inhibition at all) have been presented to 1, 2, 4 and 8 random patterns (and the corresponding number of target neurons). The network with iSTDP outperforms the network including fixed inhibition and the one with no inhibition, yielding higher recognition accuracy as shown by the average UC independently of the number of patterns/neurons (Fig. 4(a)). The network with iSTDP more accurately performs input pattern recognition,

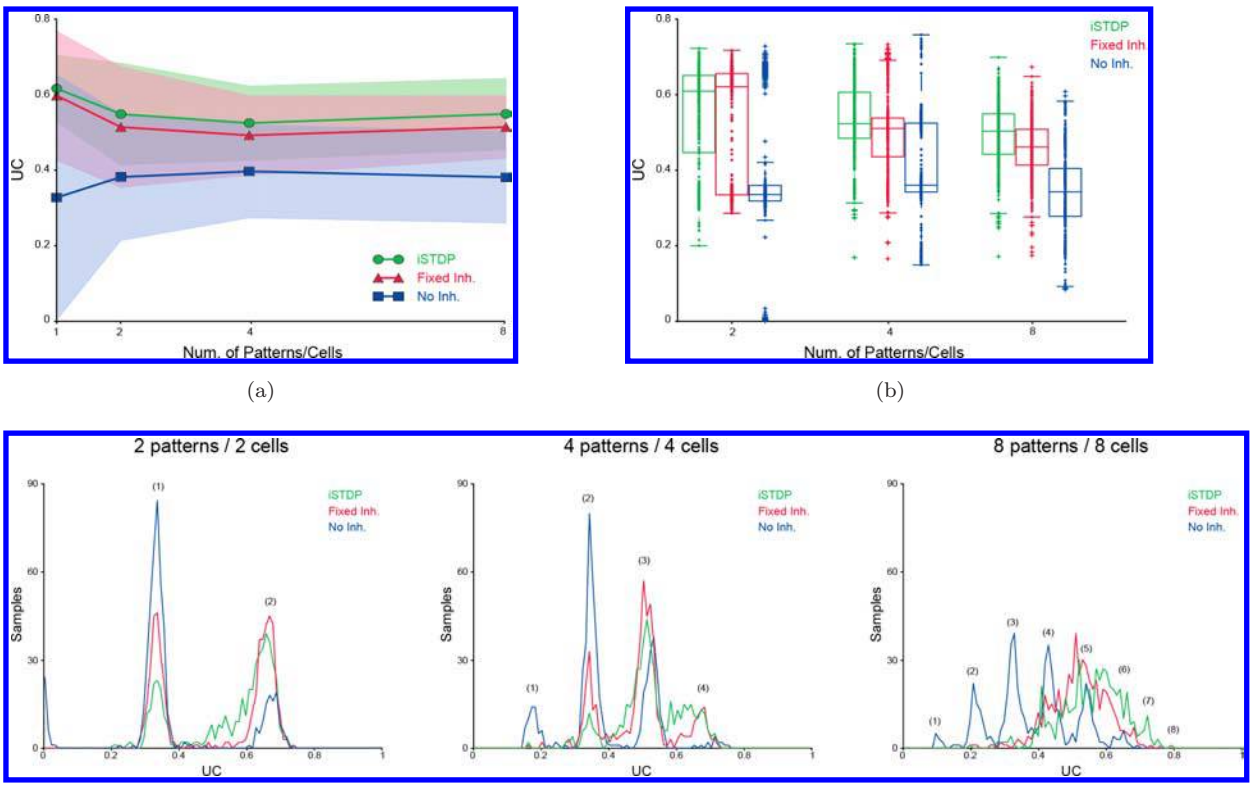

Fig. 4. (Color online) Scalability of pattern recognition performance with the number of patterns. Comparison of the network including iSTDP (green circles), fixed inhibition (red triangles) and no inhibitory connections at all (blue squares). (a) UC obtained after the learning process when 1, 2, 4 and 8 different random patterns were presented to the excitatory cells. Each point represents the average over 150 simulations with different seeds. The shadows represent the standard deviation. (b) Box-and-whisker representation of the UC obtained with 2, 4 and 8 patterns and inhibitory cells. Each box shows the first, second and third quartile of the samples, and the whiskers represent 1.5 times the inter-quartile range. The UC for each sample is marked with a dot, while the outliers are represented with a cross. (c) Histogram of the samples as a function of the UC with 2 (left), 4 (middle) and 8 (right) cells/patterns. Note that numbers have been included indicating the UC corresponding to highly accurate recognition of 1 to 8 patterns.

with the UC ranging between 0.53 (four patterns and four target cells) up to 0.62 (one pattern and one target cell).

Nevertheless, the network with fixed inhibition obtains high information transmission ratios [UC 0.03 units lower than the network configuration with iSTDP (Fig. 4(a))]. In a network lacking lateral inhibition, the target neurons are prone to respond to the same input pattern. Inserting lateral inhibition decreases the probability of different neurons to fire in the presence of the same pattern, thus enhancing the information transmission. Unluckily, fixed inhibition prevents two neurons from firing together when their respective patterns are presented simultaneously. iSTDP, as already demonstrated, overcomes this problem.

Aiming to determine the source of the difference we observed the UC obtained in the 512 samples (with different initialization seeds) that were used for the average calculation. Given the wide diversity of information transmission with each particular simulation (even when using the same network), the histogram of UC allows us to explore the distribution of particular simulations. As can be observed in the two patterns/two neurons setting (Fig. 4(c), left), the simulations are grouped around three peaks at UC values 0, 0.35 and 0.65. These peaks correspond to the cases when the network accurately recognizes to 0, 1 or 2 of the presented patterns. The presence of inhibition (e.g. fixed or iSTDP) notably reduces the number of simulations where 0 or only 1 pattern becomes recognized (Fig. 4(c), left). In particular, iSTDP effectively shifts some of the samples from 1 recognized patterns to 2 (even though some of these samples did not achieve perfect recognition as indicated by a shorter quartile box (Fig. 4(b), green box with two patterns/neurons) and the wider peak tail (Fig. 4(c), left, green line). Similar results were extracted from the four pattern/neuron configuration (Figs. 4(b) and 4(c), center). In this case, the peaks correspond to 1–3 recognized patterns with no inhibition and are shifted to 2–4 recognized patterns with fixed inhibition and iSTDP. However, the network including iSTDP achieves 3 or 4 correctly recognized patterns in a higher number of samples than the counterpart with fixed inhibition.

Finally, when the network including eight target neurons is presented with eight random patterns, similar peaks can be observed. The network with no inhibition accurately recognizes between one and six different patterns (Fig. 4(c), right). The histogram shifts to higher MT ratios by using fixed inhibition and inhibitory plasticity. The inclusion of the iSTDP mechanism leads the network to recognize up to eight of the presented patterns, although in most of the cases the network effectively recognized 5 or 6 as shown by the median and quartiles in Fig. 4(b).

3.4. *Scalability with multiple target neurons per pattern*

The network including eSTDP and iSTDP has shown to scale up with the number of patterns and it performs reasonably accurate pattern recognition. However, the results are still far from the goal of constant perfect recognition, especially with eight patterns in the input. Therefore, we wondered whether increasing the number of target neurons while keeping the number of patterns fixed (or in other words, increasing the ratio of target neurons per input pattern) would improve the ability of the network to learn and detect patterns. Thus, we have used the parameters that best performed in the four pattern/neuron test case and we have scaled up the number of inhibitory neurons from 4 up to 16 neurons. Again, the network with iSTDP has been compared with the networks including fixed inhibition and no inhibition at all.

The inclusion of additional target neurons markedly enhances the information transmission independently on the type of inhibitory synapse being used (Fig. 5(a)), achieving average values of $UC = 0.81 \pm 0.05$ (over 512 simulations) with iSTDP and 16 output cells. However, the network with iSTDP clearly outperforms the model with fixed inhibition ($UC = 0.74 \pm 0.08$) and the one with no inhibition ($UC = 0.64 \pm 0.14$).

By using eight target neurons leads the network to achieve high ratios in most of the 512 test simulations (Figs. 5(b) and 5(c), left), corresponding to all the four patterns being recognized by at least one cell. Interestingly, this setting clearly outperforms the network with only four target neurons (Fig. 4(c), center). By increasing the number of target neurons, the probability that at least one neuron becomes responsive to each pattern increases. Interestingly, the usage of iSTDP also contributes to improving

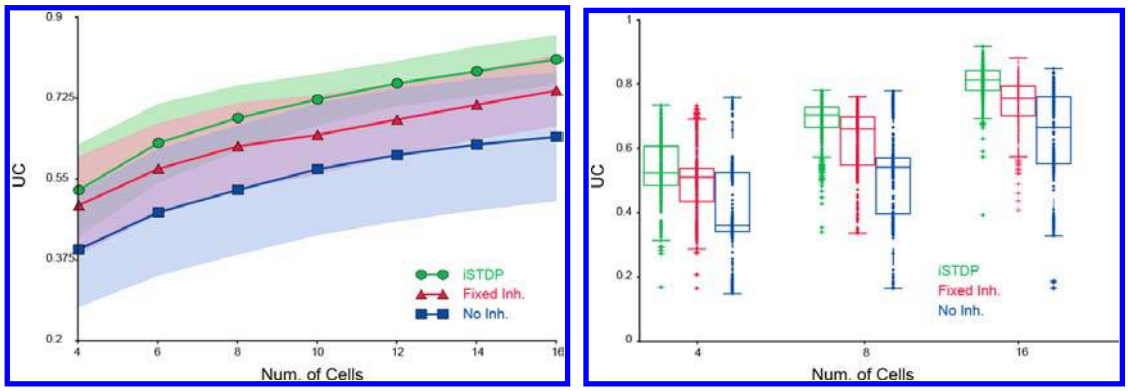

(a) (b)

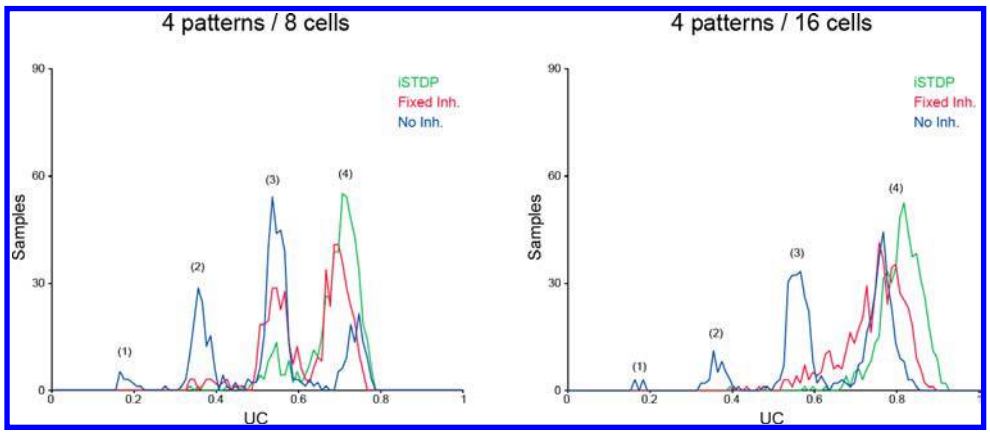

(c)

Fig. 5. (Color online) Scalability of pattern recognition performance with the number of cells. Comparison of the network including iSTDP (green circles), fixed inhibition (red triangles) and no inhibitory connections at all (blue squares). UC obtained after the learning process of four different random patterns. (a) UC obtained with networks accounting from 4 up to 16 neurons. Each point represents the average over 150 simulations with different seeds. The shadows represent the standard deviation. (b) Box-and-whisker representation of the UC obtained with 4, 8 and 16 inhibitory cells. Each box shows the first, second and third quartile of the samples, and the whiskers represent 1.5 times the inter-quartile range. The UC for each sample is marked with a dot, while the outliers are represented with a cross. (c) Histogram of the samples as a function of the obtained UC with 8 (left) and 16 (right) patterns. Note that numbers have been included indicating the UC corresponding to highly accurate recognition of 1 to 4 patterns.

the MI as evidenced with the peak distributions in Fig. 5(c), left.

Increasing the number of target neurons does not only increase the number of samples with all the input patterns being recognized, but it also increases the diversity of neuron responses which can be concluded from the shift in the peak corresponding to four recognized patterns. While this peak appears with UC $\approx$ 0.68, by using four target neurons (Fig. 4(c), center), this peak shifts to UC $\approx$ 0.72 by using eight target neurons (Fig. 5(c), left) and finally to UC $\approx$ 0.83 by using 16 target neurons. Two main reasons can explain this observation: (i) the iSTDP mechanism enables the recruitment of more than one target neuron to become responsive to each pattern but it favors the diversity in the firing phase. (ii) By using more target neurons in the network allows some of them to become redundant, thus increasing the probability of at least one neuron responding to each pattern presentation. Therefore, the inclusion of additional target neurons improves the pattern recognition performance, even in some cases where

the network with a lower number of neurons failed (e.g. patterns being presented long after the beginning of the oscillation cycle).

3.5. *The role of intrinsic plasticity and weight scaling: heterogeneous pattern recognition*

The results presented in previous paragraphs show that iSTDP plasticity in lateral connections enhances the information transmission capabilities in conjunction with plastic excitatory synapses. However, we have equipped our network with several homeostatic mechanisms (namely, intrinsic plasticity and weight scaling). Therefore, we wondered to what extent homeostatic mechanisms influence the network operation. To this aim, we have studied how the eSTDP optimal parameters ($\text{MaxWeight}_{\text{eSTDP}}$ and $r_{\text{eSTDP}}^{\text{LTD/LTP}}$) and information transmission are influenced by the selective absence of these homeostatic mechanisms. The neuron model of the target cells has been replaced by classical leaky integrate-and-fire (LIF) with the same electrical parameters as configured in our control situation. The weight scaling mechanism has been disabled and the eSTDP parameter space has been explored in the network with four target neurons (four patterns has been used to stimulate the afferent neurons). The best configuration with both homeostatic mechanisms (control case) ($\text{MaxWeight}_{\text{eSTDP}} = 1.1\,\text{nS}$, $r_{\text{eSTDP}}^{\text{LTD/LTP}} = 1.1$), the best settings with only intrinsic plasticity ($\text{MaxWeight}_{\text{eSTDP}} = 0.8\,\text{nS}$, $r_{\text{eSTDP}}^{\text{LTD/LTP}} = 1.0$) and the best configuration lacking intrinsic plasticity and weight scaling ($\text{MaxWeight}_{\text{eSTDP}} = 0.9\,\text{nS}$, $r_{\text{eSTDP}}^{\text{LTD/LTP}} = 1.4$), obtained similarly good performances ($\text{UC} = 0.53 \pm 0.1$, $\text{UC} = 0.49 \pm 0.1$, and $\text{UC} = 0.50 \pm 0.11$, respectively).

When weight scaling was enabled and intrinsic plasticity disabled, the learning performance dropped dramatically. Indeed, if the same network configuration as other case studies were used, the inhibitory neurons remained silent for the entire simulation process as occurred in the control case before the intrinsic plasticity started operating (Figs. 1(a), 1s). To make the inhibitory population become active the total sum of weights (weight-scaling parameter) was increased from 40 nS to 70 nS. Despite the re-setting of the scaling parameter, the UC of the best configuration ($\text{MaxWeight}_{\text{eSTDP}} = 0.7\,\text{nS}$, $r_{\text{eSTDP}}^{\text{LTD/LTP}} = 1.3$) remained lower ($\text{UC} = 0.21 \pm 0.04$) than in any other case study. After a close look at the simulation results, we found that the total sum of the synaptic weights was too high at the end of the simulation, forcing (due to the weight scaling) most of STDP-depressed synapses to reach higher synaptic weights than other configurations. These higher values, therefore, increased the "false alarms" and degraded the STDP selectivity.

The representation of the eSTDP parameter space evidences the role that intrinsic plasticity and weight scaling play in the network operation. Whilst the network with homeostatic mechanisms obtained high information transfer ratio with wider parameter range (see Fig. A.1(a)) ($\text{MaxWeight}_{\text{eSTDP}}$ from 0.5 nS to the maximum value 3nS and $r_{\text{eSTDP}}^{\text{LTD/LTP}}$ from 1.0 to 1.8), this range is restricted as a result of disabling the weight scaling (Fig. A.4(b)) ($\text{MaxWeight}_{\text{eSTDP}}$ from 0.5 nS to 1.2 nS and $r_{\text{eSTDP}}^{\text{LTD/LTP}}$ from 0.9 to 1.1), and disabling both intrinsic plasticity and weight scaling (Fig. A.4(c)) ($\text{MaxWeight}_{\text{eSTDP}}$ from 0.7 nS to 1.0 nS and $r_{\text{eSTDP}}^{\text{LTD/LTP}}$ from 1.3 to 1.5). On the one hand, the intrinsic plasticity avoids target neurons becoming completely silent (as a result of setting the eSTDP with high $r_{\text{eSTDP}}^{\text{LTD/LTP}}$ values) or saturated (mainly with low $r_{\text{eSTDP}}^{\text{LTD/LTP}}$ values). Weight scaling avoids synaptic weights increasing until those values where very few excitatory spikes are sufficient to elicit post-synaptic spikes (producing false positive responses). Unlike the upper bound on the eSTDP equations ($\text{MaxWeight}_{\text{eSTDP}}$ parameter), the weight scaling mechanism weighted the contribution of all the afferents that target the same neuron. Learning is then distributed along all the excitatory neurons that the pattern and the eSTDP activate". Weight scaling is also intended to avoid the case where eSTDP drives all the synapses to extremely low values.

In order to explore more deeply the role that homeostatic mechanisms play in pattern recognition, we have tested out how the ratio of afferent neurons in the pattern affects the system capability to learn and detect the patterns. Therefore, we have generated the input patterns by randomly choosing 40% (instead of the 10% we had used previously in this work) of the afferent neurons in each pattern and the eSTDP parameter space has been explored. In these experiments (in absence of intrinsic plasticity

and weight scaling) the highest MI ratio occurs with $\text{MaxWeight}_{\text{eSTDP}} = 0.3\,\text{nS}$ and $r_{\text{eSTDP}}^{\text{LTD/LTP}} = 1.4$, obtaining $\text{UC} = 0.54 \pm 0.09$ averaged over 512 simulations (Fig. A.5(a)). As expected, increasing the ratio of afferent neurons included in the pattern (and consequently the number of synapses potentiated by the eSTDP) requires the reduction of the maximum weight in the excitatory synapses. By reducing the $\text{MaxWeight}_{\text{eSTDP}}$ parameters allows that a higher number of afferent cells to be recruited by the eSTDP whilst keeping constant the total conductance that each target neuron receives when a pattern is recognized. However, it also allows the LTD/LTP ratio to be set higher (making the learning more restrictive), thus controlling the number of excitatory synapses being potentiated.

Comparing how a network with or without homeostatic mechanisms extends to a different ratio of afferent neurons in the pattern clearly shows the improvement that these mechanisms represent. The same network has been optimized to obtain the best UC as possible in four different versions: (i) including intrinsic plasticity and weight scaling (*control*), (ii) including only weight scaling (*No IP version*), (iii) including only intrinsic plasticy (*No norm* version) and (iv) disabling these two mechanisms (*No norm./IP version*). These four versions of the network have been optimized for the case where the patterns account the 10% of afferent neurons inside and the resulting configurations have been extended to different ratios of afferent neurons included. In all the experiments, the control version outperforms the ones with no intrinsic plasticity or no normalization (Fig. 6(a)). However, the difference in the UC is markedly higher when the networks are exposed to afferent ratios (in pattern) different to those used for the learning parameter adjustment. Indeed, the control network keeps reasonably good accuracy with ratios ranging from 5% of the afferents up to 100%, whilst the network lacking intrinsic plasticity and weight scaling only can learn patterns accounting the 10% of the afferents. Similar results have been found when configuring the network parameters to detect patterns accounting the 40% of afferent neurons (Fig. 6(b)). Thus, the intrinsic plasticity jointly with the weight scaling mechanism notably improves

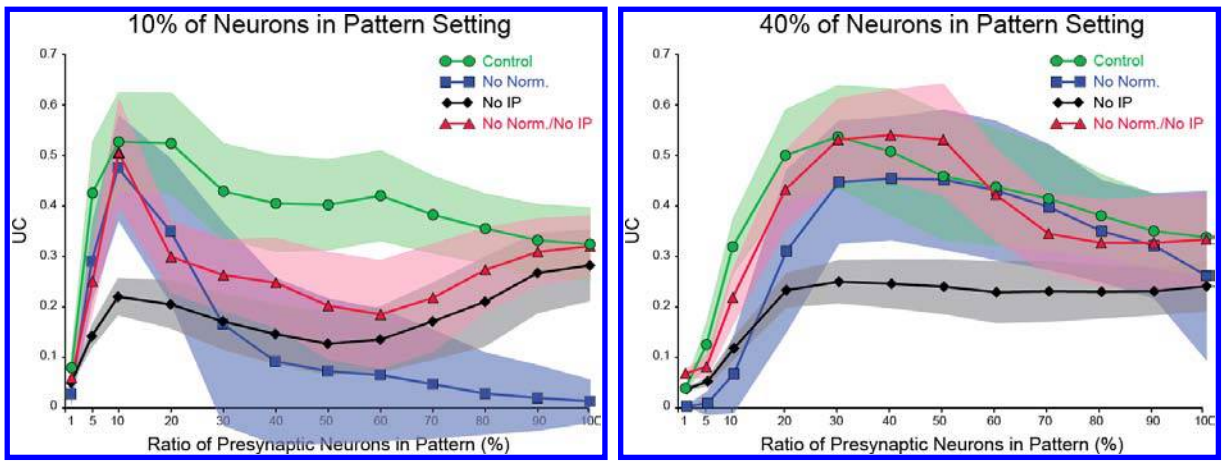

(a) (b)

Fig. 6. (Color online) Effect of the intrinsic plasticity and the weight normalization mechanism. UC obtained after 1500 s simulations in which four patterns and four inhibitory cells were used. A network with intrinsic plasticity in the inhibitory cells and weight normalization in the eSTDP connections (*control* — green) were compared to other settings without either weight scaling (*no norm* — blue) either intrinsic plasticity (no ip — gray) or none of these homeostatic mechanisms (*no norm./no ip* — red). (a) UC obtained as a function of the ratio of excitatory neurons involved in each random pattern. The eSTDP and iSTDP parameters were adjusted according to the highest UC when using the 10% of the excitatory neurons in the pattern. Each point represents the average over 150 simulations with different seeds. The shadows represent the standard deviation. (b) UC obtained as a function of the ratio of excitatory neurons involved in each random pattern. In this case, the eSTDP and iSTDP parameters were adjusted according to the highest UC when using the 40% of the excitatory neurons in the pattern.

the capability of the network to learn and recognize heterogeneous patterns within networks with different numbers of afferent neurons.

4. Discussion

This paper shows that a simple network of inhibitory interneurons with STDP both at the excitatory input synapses and at the reciprocal inhibitory synapse is sufficient to accurately learn and detect the presentation of partially overlapping and repeated input patterns. Intrinsic plasticity in the inhibitory neurons and weight scaling in the excitatory connections are needed to make the network robust to parameter changes. This ensemble of mechanisms allows the recognition of heterogeneous patterns involving between 5% and 100% of the input neurons with no need of configuration changes and we discuss the relevance of these effects for brain regulatory mechanisms and network computation.

Simulations show that eSTDP drives each target neuron to become sensitive to one of the repetitive patterns presented in the afferent neurons. In this scenario, lateral inhibition amongst the target neurons significantly enhances sparseness at the inhibitory neurons, thus preventing several target neurons from becoming sensitive to the very same pattern. These results are consistent with previous studies in *winner-takes-all* recurrent networks.[15] Our model goes one step further in pattern recognition. Our network is not just able to operate with partially overlapped patterns but also with simultaneous patterns. The presence of iSTDP in the lateral inhibitory synapses proves its worth by creating a sparse coding amongst the inhibitory neurons. On the contrary, laterally fixed inhibition, as in Ref. 15, avoids target neurons firing conjointly when several patterns are simultaneously presented at the input. Thus, the inhibitory interneurons operate as a *multiple and overlapping pattern decoder*, detecting the repetitive presence of densely-coded patterns in the excitatory afferents and creating sparse representation of those patterns. All these features enable the accurate transmission of information between the input and the target population and facilitating subsequent processing in deeper neuronal layers.

Increasing the number of inhibitory neurons effectively improved the pattern recognition capability of the network. Thus, with a number of neurons twice as large as the number of patterns, the network is able to recognize all the presented patterns in most of the tested simulations (Figs. 5(a) and 5(c)). iSTDP in the lateral inhibition was crucial for efficiently distributing the available neurons amongst the patterns presented at the input.

The simulations in this paper also make usage of previous studies by other authors showing how theta-frequency (4–8 Hz) oscillations, in conjunction with excitatory STDP can drive a single neuron to robustly detect a pattern of input currents even when a small fraction of the afferents are included in each pattern[14]. Interestingly, the presence of a reference oscillatory signal in the local field potential allows patterns of current level correlation to be transformed into phase correlation that can be efficiently processed by spike-timing learning rules.

Additionally, this study evidences that the interplay between eSTDP and iSTDP drives redundant target neurons to detect the presence of the same pattern at different phases of the oscillations, allowing the recognition of the pattern even when it was presented at a later stage of the oscillation, thus improving the information transmission as shown in Fig. 5(a). According to our simulations, certain parameter configurations of eSTDP make the target neurons elicit bursts of spikes (mainly doublets, but also some triplets) in response to the detection of a particular pattern. Our input layer is able to elicit different numbers of spikes per oscillation cycle as a phase-of-firing code does. Therefore, additional neural layers equipped with STDP could extract relevant information in a similar way to the present model.

The current model is made of LIF neurons and includes intrinsic plasticity to adjust the electrical properties of the neurons. However, it is not endowed with realistic ionic channels properties of the kind characterizing neuronal membranes and synaptic connections. Therefore, it revealed fundamental network-dependent and long-term-plasticity-dependent properties, which could then be compared with intrinsic properties of neurons and synapses. Interestingly, several neurons in the brain have experimentally been demonstrated to resonate in the theta-frequency band. This is the case of the CA1 neurons in the hippocampus[48] and the granule[49,50] and Golgi cells[51] in the input layer of the cerebellum. Realistic properties of these neurons should favor the

phase-of-firing coding in the theta-frequency band presented in this paper.

The simulations presented in this paper show that recognition of patterns including arbitrary ratios of afferent neurons can be achieved by means of the inclusion of intrinsic plasticity and synaptic weight scaling. Patterns accounting from 5% up to 100% of the afferent neurons have been effectively learned and detected with the same network configuration. Whilst intrinsic plasticity avoids target neurons becoming silent or highly active for a long time, weight scaling jointly with eSTDP distributes learning between all the afferent neurons that fire in the selected phase, thus reducing the occurrence of *false detection* spikes. Nonetheless, according to our simulations, these two mechanisms should be treated as a whole. Weight scaling demands the presence of intrinsic plasticity to cope with the variation of the weight distribution during the learning process by means of the adjustment of the neuronal electrical properties.

Intrinsic plasticity in the present model has been implemented following the equations previously proposed in Ref. 42. That model has been demonstrated to adjust not only the firing rate, but also the tuning curve of the neuron according to the actual distribution of the inputs received by the neuron.[42] In the current model, firing rate adaptation depends on the adjustment of membrane capacitance and leak conductance, reflecting the simplicity of LIF models that lack synaptic channels. However, experimental studies indicate that changes in intrinsic excitability in real neurons mainly reflect modifications of voltage gated channels.[52,53] Moreover, the inclusion of realistic firing regimes in the neuron model (such as bursting or resonance) are thought to enhance signal transmission and learning capabilities in spiking neural networks equipped with STDP.[40] Thus, the implementation of more detailed models of the neuronal excitability[54] and the integration of these models into complex learning tasks will greatly improve the understanding of the mechanisms of learning.[55]

Similarly, weight scaling has been implemented in this model by periodic normalization of the excitatory weights as previously done in the literature.[56] This simple strategy allows the neurons to remain stable as long as the STDP learning rules evolve,[24] introducing competitiveness in the synaptic inputs[57] and making the STDP learning rule less sensitive to changes in parameters.[58] Biologically speaking, excitatory postsynaptic currents have experimentally evidenced that their average amplitude increases or decreases in response to changes in the input activity.[59–61]

These simulations show that distributed synaptic plasticity strongly enhances pattern recognition capabilities of simple spiking networks driving inhibitory interneurons to recognize correlated activity. Previous studies have already evidenced that neural networks including plasticity at several synaptic layers, controlling spike-timing much better than plasticity at a single synapse[62] and effectively adapt gain in multi-layer cerebellar networks.[63] Interestingly, the simulations in this study are compatible with the learning states previously predicted for the cerebellar input layer in Ref. 62. This paper makes a further step ahead by showing how inhibitory plasticity in lateral inhibitory connections effectively complements excitatory plasticity in order to distribute the interneurons between multiple input patterns. Adding the feedback loop that typically connects excitatory neurons and interneurons can extend the network implemented here. This is the case of the loop between granule cells and Golgi cells in the cerebellum.[64] Once the interneurons become responsive to the different patterns being presented in the inputs, the inhibition of the feedback loop could effectively distribute the population of excitatory neurons to generate sparse representations of the sensorial inputs in a similar way as it has been proposed for the primary visual cortex.[20]

The results of these simulations further extend the capabilities of the interneuron beyond their traditional role of homeostatic regulators in feedback inhibitory loops. Our results confirm that inhibitory interneurons may enhance sparse coding in excitatory neurons. We have shown that both excitatory and inhibitory plasticity are fundamental to distribute different patterns amongst the whole population of interneurons. In the light of these results, revisiting the role of different interneuron networks within two well-known brain regions, such as the cerebellum (Golgi cells) or the motor cortex, must be the next challenge. Understanding how cerebellar Golgi cells can control the level of activity of excitatory granule cells[65] or how the interneurons of the motor cortex[66] can optimally control the transient dynamics of the excitatory neurons keeping the

network stable[67] are questions that our results may help to answer.

Future work will include a new layer of excitatory neurons connected by inhibitory feed-back and feed-forward pathways to our output layer. This new configuration will account for the nonlinear dynamics that is imposed by the presence of voltage-dependent conductances in the neuronal membrane. It will be interesting to explore how these network and neuron features may enhance the learning capabilities of the network even in nonsynthetic datasets.

Acknowledgments

This work was supported by Grants from the European Union (Human Brain Project, FP7-604102; CEREBSENSING, H2020-653019) to J. G., (SPIKECONTROL, H2020-658479) to N. L. and (Human Brain Project, FP7-604102) to E. D. and the University of Granada to J. G. This work was also supported by the Spanish National Grant ER (TIN2013-47069-P), partially funded by FEDER.

Appendix A. Neuron and Synapse Models

A.1. *The neuron and synapse models*

The excitatory input neurons were modeled using a current-based version of the LIF. In this neuron model, the membrane potential (V_m) is computed through the differential equation (A.1), which accounts for the effect of fast (AMPA-receptor mediated) chemical excitatory synapses and resting conductance (G_{rest}),

$$\frac{dV_m}{dt} = -\frac{(V_m - E_{\text{rest}})}{\tau_m} + \frac{I_e(t)}{C_m}, \qquad \text{(A.1)}$$

where C_m denotes the membrane capacitance, V_m is the membrane potential, E_{rest} represents the resting potential, τ_m is the membrane time constant and finally, $I_e(t)$ is the total excitatory current stimulating the neuron at a certain time t (see stimulation paragraph for a detailed explanation about the external stimulation of the neurons). These constants have been set as follows: $C_m = 2\,\text{nF}$, $E_{\text{rest}} = -70\,\text{mV}$ and $\tau_m = 10\,\text{ms}$. Every time the membrane potential overpasses the threshold potential ($E_{\text{th}} = -54\,\text{mV}$) a spike is elicited and the membrane potential is reset to E_{rest}. The refractory period (t_{ref}) has been set to 1ms and during this period the neuron membrane potential was clamped to E_{rest}.

Inhibitory neurons were modeled using a conductance-based version of the LIF model including intrinsic plasticity. The membrane potential evolution of this neuron model is described via the following equation:

$$\frac{dV_m}{dt} = r_C \cdot (-g_{\text{leak}} \cdot (V_m - E_{\text{rest}}) + I_{\text{syn}}), \qquad \text{(A.2)}$$

where V_m represents the membrane potential, E_{rest} is the resting potential, r_C and g_{leak} represent, respectively, the inverse of the membrane capacitance and the leak conductance and I_{syn} is the total current that the neuron receives through the synapses according to Eq. (A.3):

$$I_{\text{syn}} = -g_{\text{exc}} \cdot (V_m - E_{\text{exc}}) - g_{\text{inh}} \cdot (V_m - E_{\text{inh}}). \qquad \text{(A.3)}$$

E_{exc} and E_{inh} represent the reversal potential of the excitatory and inhibitory synapses and have been set to $0\,\text{mV}$ and $-80\,\text{mV}$, respectively. When the membrane potential goes above the threshold potential ($E_{\text{th}} = -50\,\text{mV}$) a spike is elicited and the membrane potential is reset to E_{rest}. The refractory period (t_{ref}) has been set to $2\,\text{ms}$. The excitatory (g_{exc}) and inhibitory (g_{inh}) conductances of a particular neuron i have been modeled using exponential functions[68] as follows:

$$\tau_{\text{exc}} \cdot \frac{dg_{\text{exc},i}}{dt} = -g_{\text{exc},i} + \sum_{k \in \text{Exc}Sp_i} w_{ji}(t_k) \cdot \delta(t - t_k), \qquad \text{(A.4)}$$

$$\tau_{\text{inh}} \cdot \frac{dg_{\text{inh}}}{dt} = -g_{\text{inh}} + \sum_{k \in \text{Inh}Sp_i} w_{ji}(t_k) \cdot \delta(t - t_k), \qquad \text{(A.5)}$$

where τ_{exc} and τ_{inh} represent the excitatory and inhibitory time constants and have been set to $0.5\,\text{ms}$ and $10\,\text{ms}$ respectively, $\text{ExcSp}_i/\text{InhSp}_i$ is the set of the spikes reaching the neuron i through the excitatory/inhibitory afferent synapses and $\delta(t)$ is the Dirac delta function. According to these equations, every time a spike is received (at time t_k) through an excitatory or inhibitory connection (linking the presynaptic neuron j and the postsynaptic neuron i), the excitatory or inhibitory conductance is increased accordingly to the synaptic weight existing in that synapse (w_{ji}). For simplicity, these equations consider both excitatory and inhibitory conductances and synaptic weights to be positive or zero.

The equations of the intrinsic plasticity mechanism have been included in Sec. 2.2.1.

A.2. *Spike-Time dependent plasticity*

The weights of the excitatory synapses (those connecting the stimulation fibers with the inhibitory neurons) have been implemented following classical additive eSTDP. According to this type of Hebbian plasticity, LTP is produced when a postsynaptic spike is elicited shortly after a presynaptic spike. Inversely, a presynaptic spike following a postsynaptic spike will generate LTD (Fig. 1(c)). The equations governing the weight change are as follows:

$$\Delta w = \begin{cases} A^{\mathrm{LTP}}_{\mathrm{eSTDP}} \cdot e^{-\frac{t_{\mathrm{post}} - t_{\mathrm{pre}}}{\tau^{+}_{\mathrm{eSTDP}}}} & \text{if } t_{\mathrm{post}} \geq t_{\mathrm{pre}}, \\ A^{\mathrm{LTD}}_{\mathrm{eSTDP}} \cdot e^{-\frac{t_{\mathrm{pre}} - t_{\mathrm{post}}}{\tau^{-}_{\mathrm{eSTDP}}}} & \text{otherwise,} \end{cases} \tag{A.6}$$

where $\tau^{+}_{\mathrm{eSTDP}}$ and $\tau^{-}_{\mathrm{eSTDP}}$ are the time constants of the potentiation and depression components and have been set to 16.8 ms and 33.7 ms, respectively. The t_{post} and t_{pre} variables refer to the time when the postsynaptic and presynaptic spikes happen. An all-to-all implementation of this eSTDP has been used, so that all the previous spikes have been considered in order to calculate the total amount of LTD and LTP produced. The maximum amount of LTP ($A^{\mathrm{LTP}}_{\mathrm{eSTDP}}$) being produced after two (one presynaptic and one postsynaptic) coincident spikes has been set to $A^{\mathrm{LTP}}_{\mathrm{eSTDP}} = 3 \cdot 10^{-3} \cdot \mathrm{MaxWeight}_{\mathrm{eSTDP}}$ while the maximum amount of LTD ($A^{\mathrm{LTD}}_{\mathrm{eSTDP}}$) has been adjusted in relation to the amount of LTP according to $A^{\mathrm{LTD}}_{\mathrm{eSTDP}} = r^{\mathrm{LTD/LTP}}_{\mathrm{eSTDP}} \cdot A^{\mathrm{LTP}}_{\mathrm{eSTDP}}$. The influence of $\mathrm{MaxWeight}_{\mathrm{eSTDP}}$ and $r^{\mathrm{LTD/LTP}}_{\mathrm{eSTDP}}$ parameters have been analyzed throughout this paper in different conditions and their values have been adjusted with the aim of achieving the highest information transmission between the input layer and the inhibitory cells (see MI section below).

References

1. T. V. Bliss and G. L. Collingridge, A synaptic model of memory: Long-term potentiation in the hippocampus, *Nature* **361** (1993) 31–39.
2. E. D'Angelo, Homeostasis of intrinsic excitability: Making the point, *J. Physiol.* **588** (2010) 901–902.
3. D. J. Linden, The return of the spike postsynaptic action potentials and the induction of LTP and LTD, *Neuron* **22** (1999) 661–666.
4. R. S. Petersen, S. Panzeri and M. Maravall, Neural coding and contextual influences in the whisker system, *Biol. Cybern.* **100** (2009) 427–446.
5. S. Eldawlatly and K. G. Oweiss, Millisecond-timescale local network coding in the rat primary somatosensory cortex, *PLoS One* **6**(6) (2011) e21649.
6. R. D. S. Raizada and S. Grossberg, Towards a theory of the laminar architecture of cerebral cortex: Computational clues from the visual system, *Cereb. Cortex* **13** (2003) 100–113.
7. H. Ko, L. Cossell, C. Baragli, J. Antolik, C. Clopath, S. B. Hofer and T. D. Mrsic-Flogel, The emergence of functional microcircuits in visual cortex, *Nature* **496** (2013) 96–100.
8. J. P. Gavornik and M. F. Bear, Learned spatiotemporal sequence recognition and prediction in primary visual cortex, *Nat. Neurosci.* **17** (2014) 732–737.
9. N. Caporale and Y. Dan, Spike timing-dependent plasticity: A Hebbian learning rule, *Annu. Rev. Neurosci.* **31** (2008) 25–46.
10. H. Markram, J. Lübke, M. Frotscher and B. Sakmann, Regulation of synaptic efficacy by coincidence of postsynaptic APs and EPSPs, *Science* **275** (1997) 213–215.
11. G. Q. Bi and M. M. Poo, Synaptic modifications in cultured hippocampal neurons: Dependence on spike timing, synaptic strength, and postsynaptic cell type, *J. Neurosci.* **18** (1998) 10464–10472.
12. D. E. Feldman, Timing-based LTP and LTD at vertical inputs to layer II/III pyramidal cells in rat barrel cortex, *Neuron* **27** (2000) 45–56.
13. T. Masquelier, R. Guyonneau and S. J. Thorpe, Spike timing dependent plasticity finds the start of repeating patterns in continuous spike trains, *PLoS One* **3** (2008) e1377.
14. T. Masquelier, E. Hugues, G. Deco and S. J. Thorpe, Oscillations, phase-of-firing coding, and spike timing-dependent plasticity: An efficient learning scheme, *J. Neurosci.* **29** (2009) 13484–13493.
15. T. Masquelier, R. Guyonneau and S. J. Thorpe, Competitive STDP-based spike pattern learning, *Neural Comput.* **21** (2009) 1259–1276.
16. T. Samura and M. Hattori, Hippocampal memory modification induced by pattern completion and spike-timing dependent synaptic plasticity, *Int. J. Neural Syst.* **15** (2005) 13–22.
17. J. A. D'amour and R. C. Froemke, Inhibitory and excitatory spike-timing-dependent plasticity in the auditory cortex, *Neuron* **86** (2015) 514–528.
18. T. P. Vogels, H. Sprekeler, F. Zenke, C. Clopath and W. Gerstner, Inhibitory plasticity balances excitation and inhibition in sensory pathways and memory networks, *Science* **334** (2011) 1569–1573.
19. F. I. Kleberg, T. Fukai and M. Gilson, Excitatory and inhibitory STDP jointly tune feedforward neural circuits to selectively propagate correlated spiking activity, *Front. Comput. Neurosci.* **8** (2014) 53.
20. P. D. King, J. Zylberberg and M. R. DeWeese, Inhibitory interneurons decorrelate excitatory cells to drive sparse code formation in a spiking model of V1, *J. Neurosci.* **33** (2013) 5475–5485.

21. M. Badoual, Q. Zou, A. P. Davison, M. Rudolph, T. Bal, Y. Frégnac and A. Destexhe, Biophysical and phenomenological models of multiple spike interactions in spike-timing dependent plasticity, *Int. J. Neural Syst.* **16** (2006) 79–97.
22. T. J. Strain, L. J. McDaid, T. M. McGinnity, L. P. Maguire and H. M. Sayers, An stdp training algorithm for a spiking neural network with dynamic threshold neurons, *Int. J. Neural Syst.* **20** (2010) 463–480.
23. A. J. Watt and N. S. Desai, Homeostatic plasticity and STDP: Keeping a neuron's cool in a fluctuating world, *Front. Synaptic Neurosci.* **2** (2010) 5.
24. C. Tetzlaff, C. Kolodziejski, M. Timme and F. Wörgötter, Synaptic scaling in combination with many generic plasticity mechanisms stabilizes circuit connectivity, *Front. Comput. Neurosci.* **5** (2011) 47.
25. M. E. Lambo and G. G. Turrigiano, Synaptic and intrinsic homeostatic mechanisms cooperate to increase L2/3 pyramidal neuron excitability during a late phase of critical period plasticity, *J. Neurosci.* **33** (2013) 8810–8819.
26. G. Turrigiano, L. F. Abbott and E. Marder, Activity-dependent changes in the intrinsic properties of cultured neurons, *Science* **264** (1994) 974–977.
27. N. S. Desai, Homeostatic plasticity in the CNS: Synaptic and intrinsic forms, *J. Physiol. Paris* **97** (2003) 391–402.
28. P. Yger and M. Gilson, Models of metaplasticity: A review of concepts, *Front. Comput. Neurosci.* **9** (2015) 1–14.
29. S. Tolu, M. Vanegas, J. A. Garrido, N. R. Luque and E. Ros, Adaptive and predictive control of a simulated robot arm, *Int. J. Neural Syst.* **23** (2013) 1350010.
30. N. R. Luque, J. A. Garrido, R. R. Carrillo, S. Tolu and E. Ros, Adaptive cerebellar spiking model embedded in the control loop: Context switching and robustness against noise, *Int. J. Neural Syst.* **21** (2011) 385.
31. N. R. Luque, J. A. Garrido, R. R. Carrillo, O. J.-M. D. Coenen and E. Ros, Cerebellar like corrective model inference engine for manipulation tasks, *IEEE Trans. Syst. Man. Cybern. B. Cybern.* **41** (2011) 1299–1312.
32. S. Ghosh-Dastidar and H. Adeli, A new supervised learning algorithm for multiple spiking neural networks with application in epilepsy and seizure detection, *Neural Networks* **22** (2009) 1419–1431.
33. S. Ghosh-Dastidar and H. Adeli, Improved spiking neural networks for EEG classification and epilepsy and seizure detection, *Integr. Comput. Aided. Eng.* **14** (2007) 187–212.
34. G. Zhang, H. Rong, F. Neri and M. J. Pérez-Jiménez, An optimization spiking neural P system for approximately solving combinatorial optimization problems, *Int. J. Neural Syst.* **24** (2014) 1440006.
35. N. R. Luque, J. A. Garrido, J. Ralli, J. J. Laredo and E. Ros, From sensors to spikes: Evolving receptive fields to enhance sensorimotor information in a robot-arm, *Int. J. Neural Syst.* **22** (2012) 1250013.
36. J. Friedrich, R. Urbanczik and W. Senn, Code-specific learning rules improve action selection by populations of spiking neurons, *Int. J. Neural Syst.* **24** (2014) 1450002.
37. J. L. Rosselló, V. Canals, A. Oliver and A. Morro, Studying the role of synchronized and chaotic spiking neural ensembles in neural information processing, *Int. J. Neural Syst.* **24** (2014) 1430003.
38. S. Shapero, M. Zhu, J. Hasler and C. Rozell, Optimal sparse approximation with integrate and fire neurons, *Int. J. Neural Syst.* **24** (2014) 1440001.
39. S. Ghosh-Dastidar and H. Adeli, Spiking neural networks, *Int. J. Neural Syst.* **19** (2009) 295–308.
40. S. Nobukawa and H. Nishimura, Enhancement of spike-timing-dependent plasticity in spiking neural systems with noise, *Int. J. Neural Syst.* **26** (2015) 1550040.
41. W. Gerstner and W. Kistler, *Spiking Neuron Models*: *Single Neurons*, *Populations*, *Plasticity* (Cambridge University Press, 2002).
42. C. Li and Y. Li, A spike-based model of neuronal intrinsic plasticity, *IEEE Trans. Auton. Ment. Dev.* **5** (2013) 62–73.
43. M. A. Woodin, K. Ganguly and M. M. Poo, Coincident pre- and postsynaptic activity modifies GABAergic synapses by postsynaptic changes in Cl- transporter activity, *Neuron* **39** (2003) 807–820.
44. M. O. Gewaltig and M. Diesmann, NEST (Neural Simulation Tool), *Scholarpedia* **2** (2007) 1430.
45. P. E. Latham and Y. Roudi, Mutual information, *Scholarpedia* **4** (2009) 1658.
46. W. H. Press, S. A. Teukolsky, W. T. Vetterling and B. P. Flannery, *Numerical Recipes*: *The Art of Scientific Computing*, 3rd edn. (Cambridge University Press, Cambridge, 2007).
47. J. M. Eppler, M. Helias, E. Muller, M. Diesmann and M.-O. Gewaltig, PyNEST: A convenient interface to the NEST simulator, *Front. Neuroinform.* **2** (2008) 12.
48. L. S. Leung and H. W. Yu, Theta-frequency resonance in hippocampal CA1 neurons *in vitro* demonstrated by sinusoidal current injection, *J. Neurophysiol.* **79** (1998) 1592–1596.
49. E. D'Angelo, T. Nieus, A. Maffei, S. Armano, P. Rossi, V. Taglietti, A. Fontana and G. Naldi, Theta-frequency bursting and resonance in cerebellar granule cells: Experimental evidence and modeling of a slow k+-dependent mechanism, *J. Neurosci.* **21** (2001) 759–770.
50. D. Gandolfi, P. Lombardo, J. Mapelli, S. Solinas and E. D'Angelo, θ-frequency resonance at the cerebellum input stage improves spike timing on

the millisecond time-scale, *Front. Neural Circuits* **7** (2013) 64.
51. S. Solinas, L. Forti, E. Cesana, J. Mapelli, E. De Schutter and E. D'Angelo, Fast-reset of pacemaking and theta-frequency resonance patterns in cerebellar golgi cells: Simulations of their impact *in vivo*, *Front. Cell. Neurosci.* **1** (2007) 4.
52. N. S. Desai, L. C. Rutherford and G. G. Turrigiano, Plasticity in the intrinsic excitability of cortical pyramidal neurons, *Nat. Neurosci.* **2** (1999) 515–520.
53. W. Zhang and D. J. Linden, The other side of the engram: Experience-driven changes in neuronal intrinsic excitability, *Nat. Rev. Neurosci.* **4** (2003) 885–900.
54. Z. Wang, L. Guo and M. Adjouadi, A generalized leaky integrate-and-fire neuron model with fast implementation method, *Int. J. Neural Syst.* **24** (2014) 1440004.
55. E. D'Angelo, S. Solinas, J. Garrido, C. Casellato, A. Pedrocchi, J. Mapelli, D. Gandolfi and F. Prestori, Realistic modeling of neurons and networks: Towards brain simulation, *Funct. Neurol.* **28** (2013) 153–166.
56. C. Savin, P. Joshi and J. Triesch, Independent component analysis in spiking neurons, *PLoS Comput. Biol.* **6** (2010) e1000757.
57. M. C. van Rossum, G. Q. Bi and G. G. Turrigiano, Stable Hebbian learning from spike timing-dependent plasticity, *J. Neurosci.* **20** (2000) 8812–8821.
58. G. Turrigiano, The self-tuning neuron: Synaptic scaling of excitatory synapses, *Cell* **135** (2008) 422–435.
59. G. G. Turrigiano and S. B. Nelson, Homeostatic plasticity in the developing nervous system, *Nat. Rev. Neurosci.* **5** (2004) 97–107.
60. A. J. Watt, M. C. van Rossum, K. M. MacLeod, S. B. Nelson and G. G. Turrigiano, Activity coregulates quantal AMPA and NMDA currents at neocortical synapses, *Neuron* **26** (2000) 659–670.
61. G. G. Turrigiano, K. R. Leslie, N. S. Desai, L. C. Rutherford and S. B. Nelson, Activity-dependent scaling of quantal amplitude in neocortical neurons, *Nature* **391** (1998) 892–896.
62. J. A. Garrido, E. Ros and E. D'Angelo, Spike timing regulation on the millisecond scale by distributed synaptic plasticity at the cerebellum input stage: A simulation study, *Front. Comput. Neurosci.* **7** (2013) 64.
63. J. A. Garrido, N. R. Luque, E. D'Angelo and E. Ros, Distributed cerebellar plasticity implements adaptable gain control in a manipulation task: A closed-loop robotic simulation, *Front. Neural Circuits* **7** (2013) 159.
64. E. D'Angelo, S. K. E. Koekkoek, P. Lombardo, S. Solinas, E. Ros, J. Garrido, M. Schonewille and C. I. De Zeeuw, Timing in the cerebellum: Oscillations and resonance in the granular layer, *Neuroscience* **162** (2009) 805–815.
65. M. Ito, Cerebellar circuitry as a neuronal machine, *Prog. Neurobiol.* **78** (2006) 272–303.
66. B. Strack, K. M. Jacobs and K. J. Cios, Simulating vertical and horizontal inhibition with short-term dynamics in a multi-column multi-layer model of neocortex, *Int. J. Neural Syst.* **24** (2014) 1440002.
67. G. Hennequin, T. P. Vogels and W. Gerstner, Optimal control of transient dynamics in balanced networks supports generation of complex movements, *Neuron* **82** (2014) 1394–1406.
68. A. Roth and M. C. W. van Rossum, Modeling synapses, in *Computational Model Methods Neuroscience* (MIT Press, 2009), pp. 139–160.

Supplementary Figures

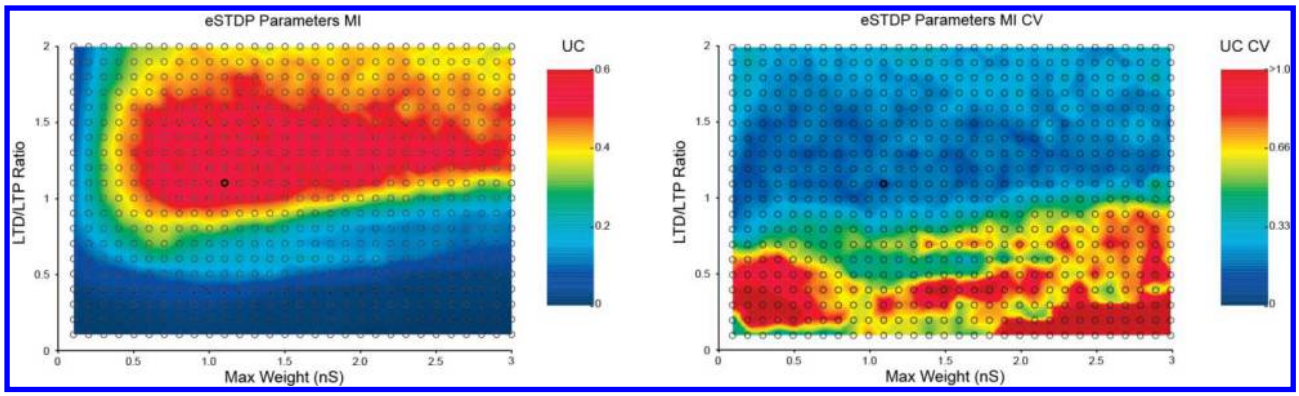

(a)

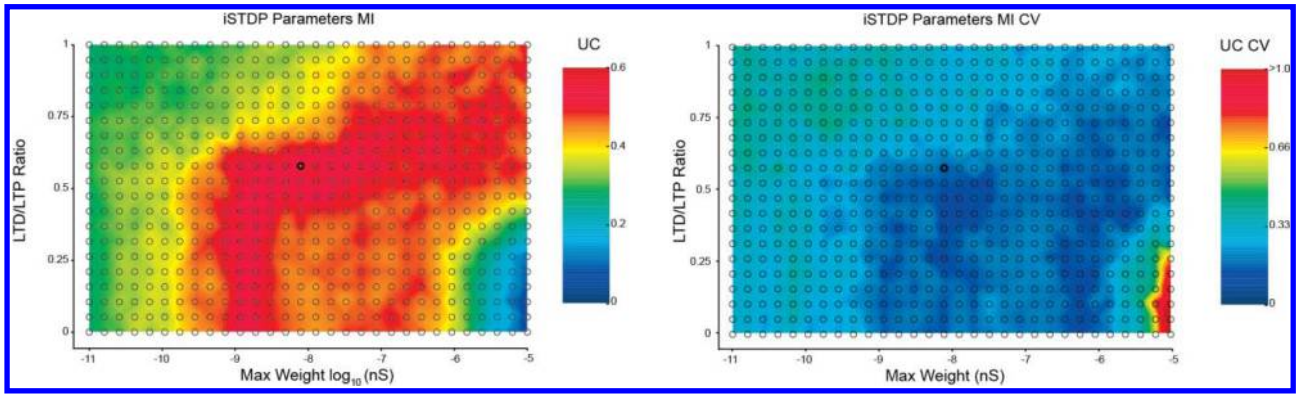

(b)

Fig. A.1. eSTDP and iSTDP plasticity parameter exploration with four inhibitory neurons and four patterns with iSTDP between the inhibitory neurons. Each circle represents the average over 30 simulations and the best performing setting has been highlighted in bold. (a) Average of the UC (left) and CV (right) obtained as a function of the eSTDP parameters: ($\text{MaxWeight}_{\text{eSTDP}}$ —x-axis) and LTD/LTP ratio ($r_{\text{eSTDP}}^{\text{LTD/LTP}}$ —y-axis). (b) UC (left) and CV (right) obtained as a function of the iSTDP parameters: ($\text{MaxWeight}_{\text{iSTDP}}$ —x-axis) and LTD/LTP ratio ($r_{\text{iSTDP}}^{\text{LTD/LTP}}$ —y-axis).

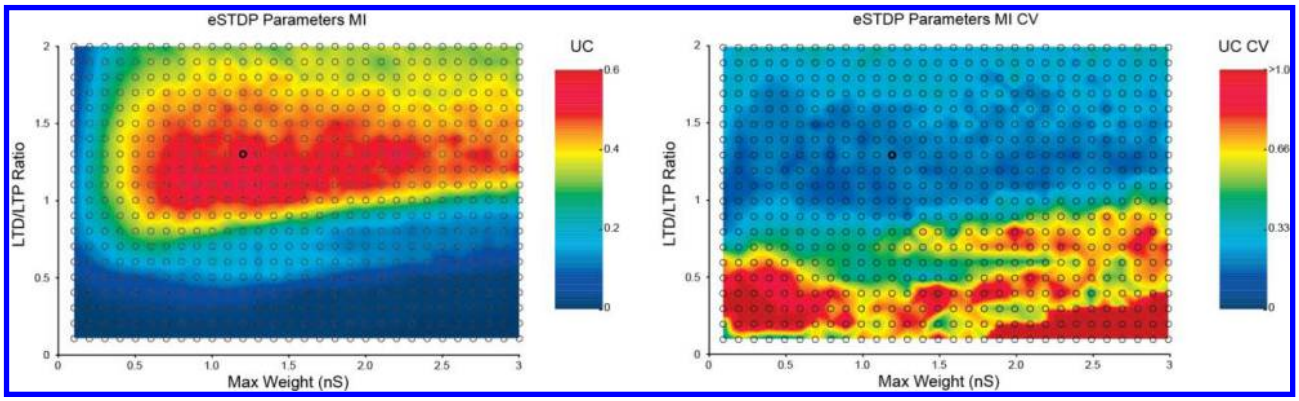

(a)

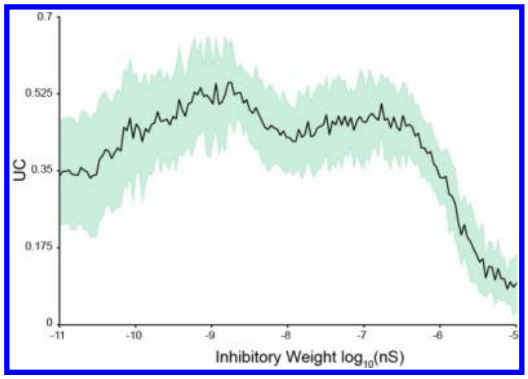

(b)

Fig. A.2. eSTDP plasticity and inhibitory weight parameter exploration with four inhibitory neurons and four patterns with fixed inhibition between the inhibitory neurons. Each circle represents the average over 30 simulations and the best performing setting has been highlighted in bold. (a) Average of the UC (left) and CV (right) obtained as a function of the eSTDP parameters: ($\text{MaxWeight}_{\text{eSTDP}}$ —x-axis) and LTD/LTP ratio ($r_{\text{eSTDP}}^{\text{LTD/LTP}}$ —y-axis). (b) UC as a function of the inhibitory weight between the inhibitory cells.

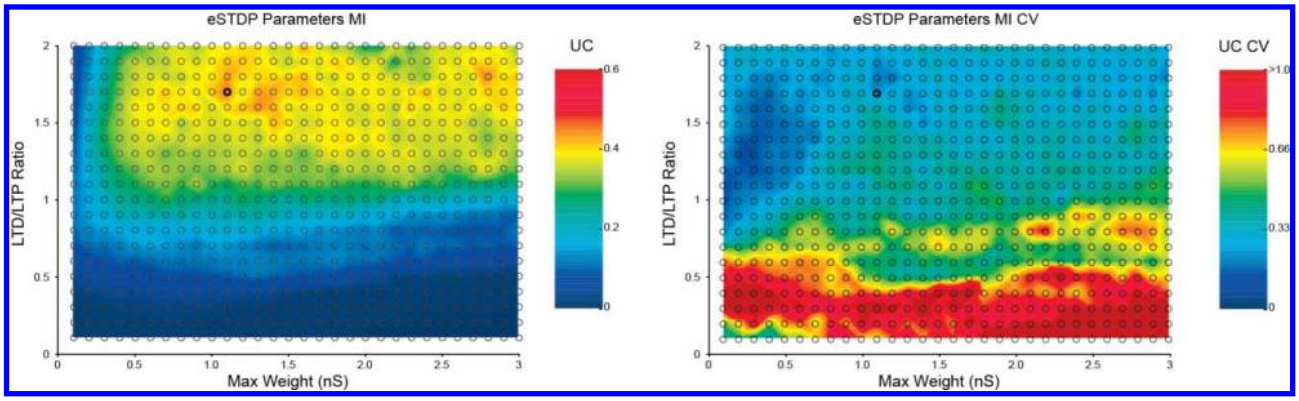

Fig. A.3. eSTDP plasticity weight parameter exploration with four inhibitory neurons and four patterns with no inhibition between the inhibitory cells. Each circle represents the average over 30 simulations and the best performing setting has been highlighted in bold. (a) Average of the UC (left) and CV (right) obtained as a function of the eSTDP parameters: ($\text{MaxWeight}_{\text{eSTDP}}$ —x-axis) and LTD/LTP ratio ($r_{\text{eSTDP}}^{\text{LTD/LTP}}$ —y-axis).

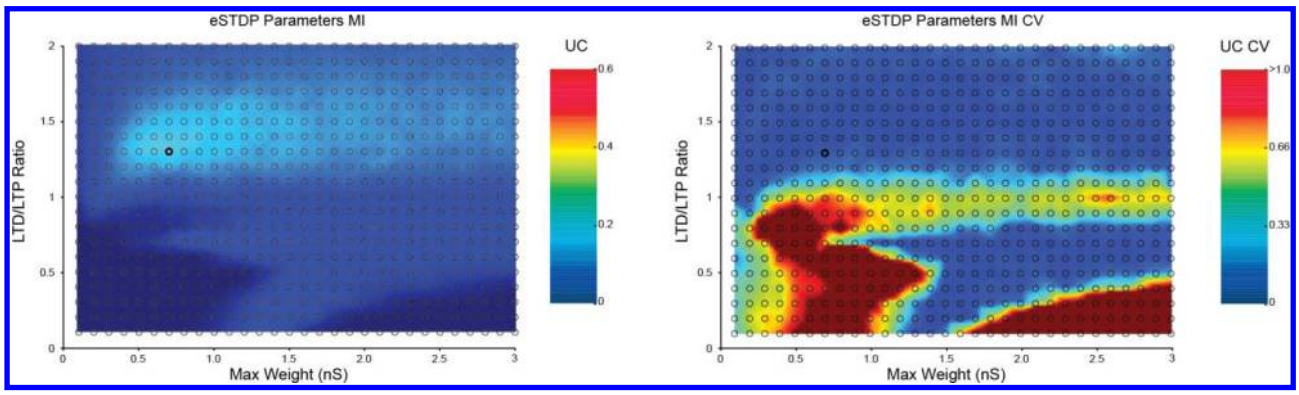

(a)

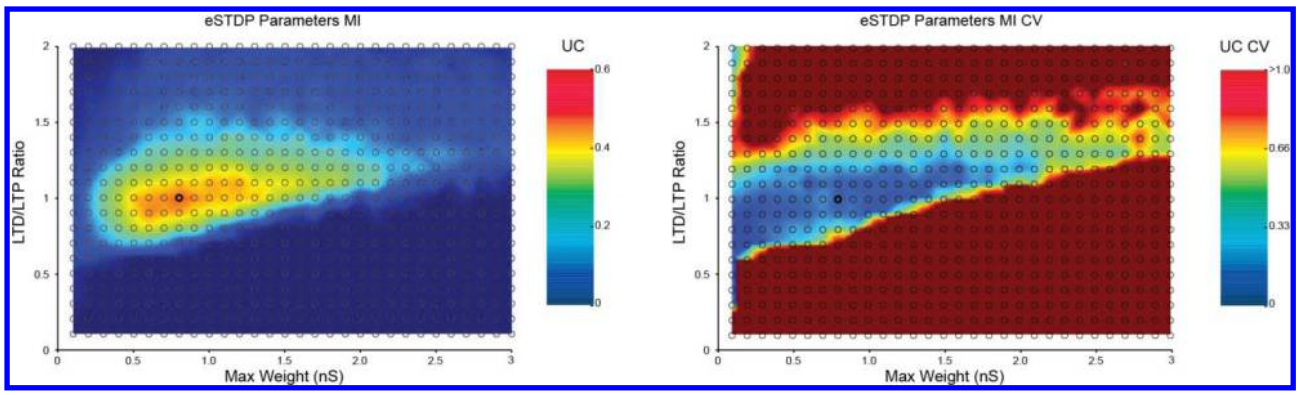

(b)

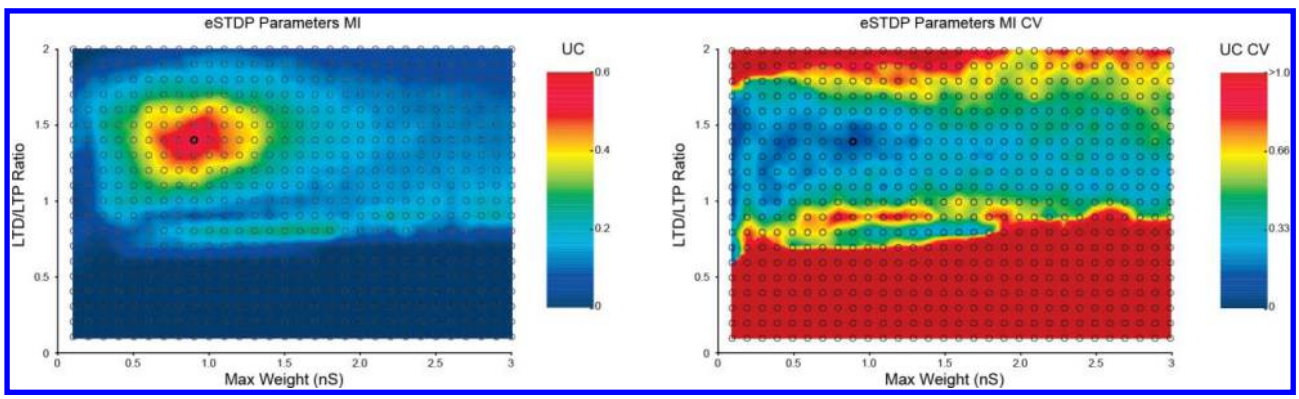

(c)

Fig. A.4. eSTDP plasticity parameter exploration with four inhibitory neurons, four patterns and 10% percent of the excitatory neurons included in each pattern. Each circle represents the average over 20 simulations and the best performing setting has been highlighted in bold. Average of the UC (left) and CV (right) obtained as a function of the eSTDP parameters: ($\text{MaxWeight}_{\text{eSTDP}}$ —x-axis) and LTD/LTP ratio ($r_{\text{eSTDP}}^{\text{LTD/LTP}}$ —y-axis) in a network with: (a) only weight scaling, (b) only intrinsic plasticity and (c) neither intrinsic plasticity nor weight scaling.

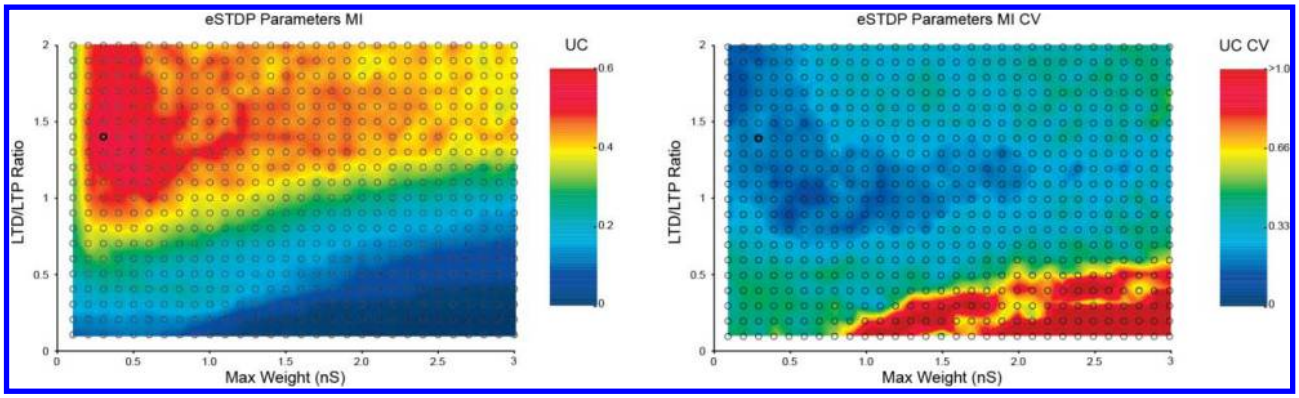

(a)

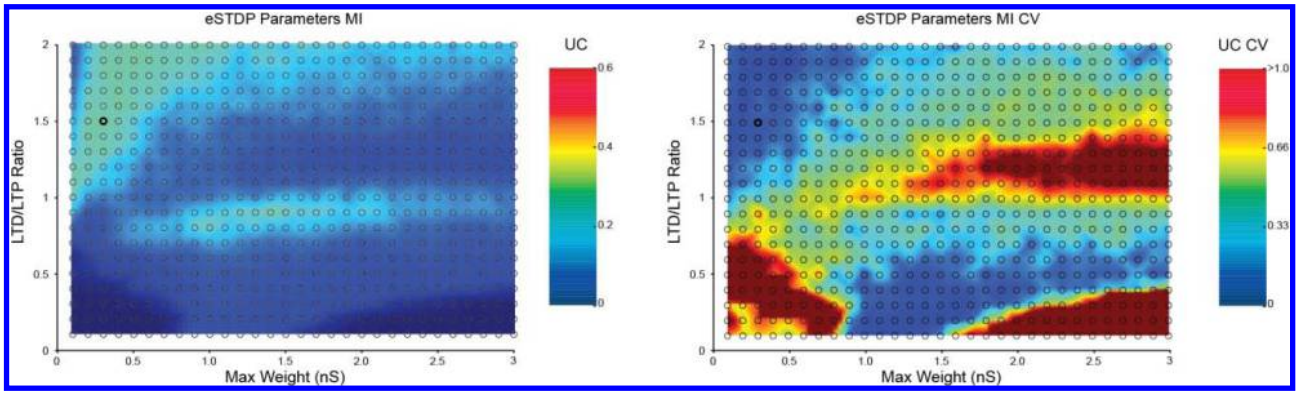

(b)

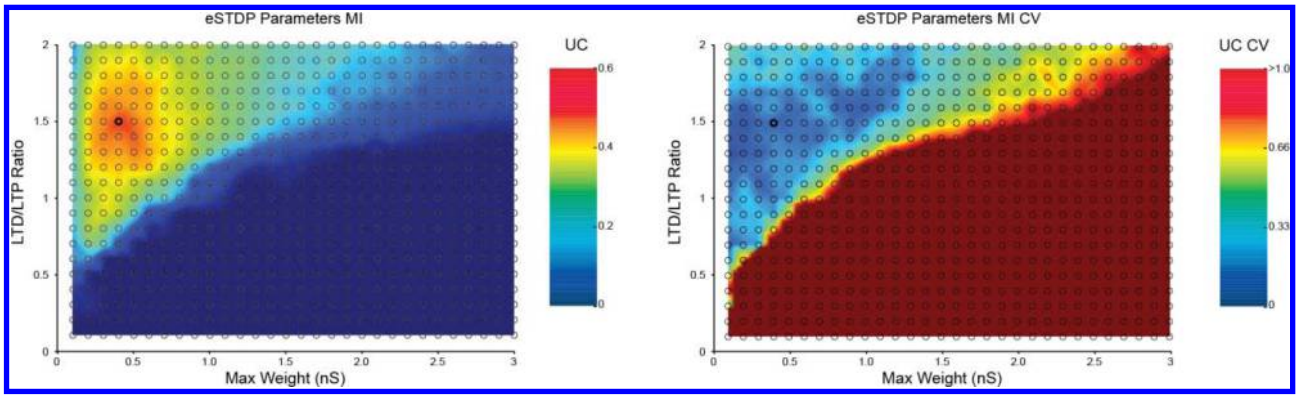

(c)

Fig. A.5. eSTDP plasticity parameter exploration with four inhibitory neurons, four patterns and 40% of excitatory neurons included in each pattern. Each circle represents the average over 20 simulations and the best performing setting has been highlighted in bold. Average of the UC (left) and CV (right) obtained as a function of the eSTDP parameters: ($\text{MaxWeight}_{\text{eSTDP}}$ —x-axis) and LTD/LTP ratio ($r_{\text{eSTDP}}^{\text{LTD/LTP}}$ —y-axis) in a network with: (a) both intrinsic plasticity and weight scaling, (b) only weight scaling, (c) only intrinsic plasticity and (d) neither intrinsic plasticity nor weight scaling.

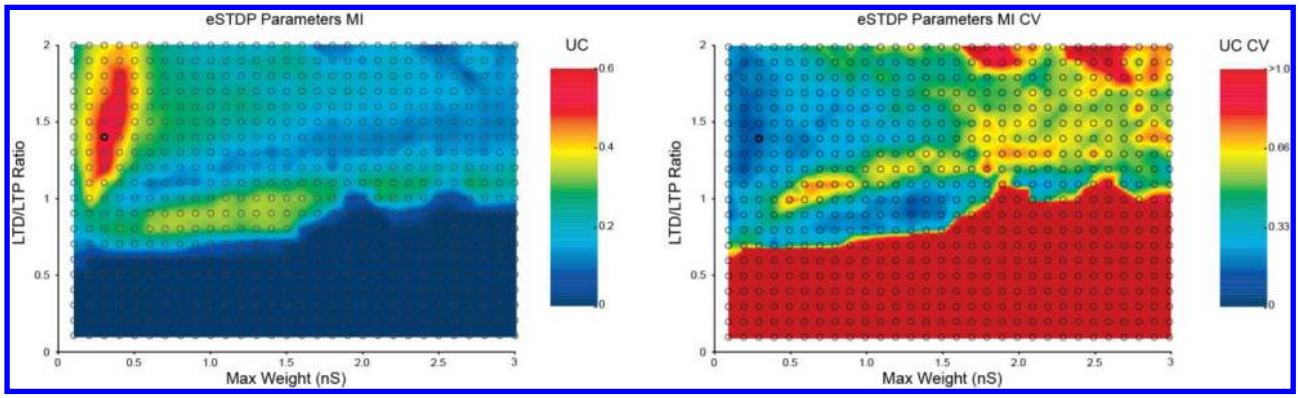

(d)

Fig. A.5. (*Continued*)